

The Carotid Body Detects Circulating Tumor Necrosis Factor-Alpha to Activate a Sympathetic Anti-Inflammatory Reflex

Pedro L. Katayama¹, Isabela P. Leirão¹, Alexandre Kanashiro², João Paulo M. Luiz³, Fernando Q. Cunha³, Luiz C. C. Navegantes⁴, Jose V. Menani¹, Daniel B. Zoccal¹, Débora S. A. Colombari¹ & Eduardo Colombari¹

Affiliations

¹Department of Physiology and Pathology, School of Dentistry, São Paulo State University, Araraquara, São Paulo, Brazil.

²Department of Neurosciences and Behavior, Ribeirão Preto Medical School, University of São Paulo, Ribeirão Preto, São Paulo, Brazil

³Department of Pharmacology, Ribeirão Preto Medical School, University of São Paulo, Ribeirão Preto, São Paulo, Brazil.

⁴Department of Physiology, Ribeirão Preto Medical School, University of São Paulo, Ribeirão Preto, São Paulo, Brazil.

Corresponding authors

Pedro L. Katayama & Eduardo Colombari
Department of Physiology and Pathology, School of Dentistry, São Paulo State University, Rua Humaita, 1680, Centro, Araraquara/SP, Brazil – Postal code: 14801-903. emails: katayamapl@gmail.com; eduardo.colombari@unesp.br

39 **Abstract**

40 Recent evidence has suggested that the carotid bodies might act as immunological
41 sensors, detecting pro-inflammatory mediators and signalling to the central nervous
42 system, which, in turn, orchestrates autonomic responses. Here, we demonstrated
43 that the TNF- α receptor type I is expressed in the carotid bodies of rats. The systemic
44 administration of TNF- α increased carotid body afferent discharge and activated
45 glutamatergic neurons in the nucleus tractus solitarius (NTS) that project to the rostral
46 ventrolateral medulla (RVLM), where the majority of pre-sympathetic neurons reside.
47 The activation of these neurons was accompanied by generalized activation of the
48 sympathetic nervous system. Carotid body ablation blunted the TNF- α -induced
49 activation of RVLM-projecting NTS neurons and the increase in splanchnic
50 sympathetic nerve activity. Finally, plasma and spleen levels of cytokines after TNF- α
51 administration were higher in rats subjected to either carotid body ablation or
52 splanchnic sympathetic denervation. Collectively, our findings indicate that the carotid
53 body detects circulating TNF- α to activate a counteracting sympathetic anti-
54 inflammatory mechanism.

55

56 **Keywords:** Carotid Body; Sympathetic Nervous System; Inflammation; Neuroimmune
57 Interactions; Neuroimmunomodulation; Neural Circuits

58

59

60

61

62

63

64

65

66

67

68

69

70

71

72 **Introduction**

73 The existence of neuroimmune interactions and their relevance to the control of
74 inflammation are well-established and have been extensively explored in the last 20
75 years (Abe et al., 2017; Bassi et al., 2020; Filiano et al., 2016; Kressel et al., 2020;
76 Lankadeva et al., 2020; Martelli et al., 2014; Mughrabi et al., 2021; Murray et al., 2021;
77 Steinman, 2004; Tanaka et al., 2021) since the discovery of the “inflammatory reflex”
78 (Borovikova et al., 2000). In general, there is a consensus that this reflex works as a
79 negative-feedback mechanism that comprises: 1) a detection component, which
80 identifies pathogen- or danger-associated molecular patterns, generating an
81 inflammatory response; 2) an afferent arm, which conveys information about the
82 systemic inflammatory status to the central nervous system; 3) integrative centers in
83 the brain, that receive and process signals regarding the systemic inflammatory
84 condition, orchestrating an appropriate counteracting response and; 4) an efferent
85 arm, which are the effectors that exert immunomodulatory functions to promote
86 resolution of infection and inflammation.

87 The vagus nerve is considered an important element in neuroimmune
88 interactions (Borovikova et al., 2000; Kressel et al., 2020; Mughrabi et al., 2021). Its
89 afferent (sensory) and efferent (motor) fibers are involved in the bidirectional
90 communication between the nervous and the immune systems, providing a reflex
91 mechanism known as the “cholinergic anti-inflammatory pathway” (Borovikova et al.,
92 2000; Mughrabi et al., 2021). According this mechanism, vagal sensory neurons detect
93 inflammatory mediators produced in conditions of systemic inflammation and send this
94 information to the central nervous system (Watkins et al., 1995), which, in turn,
95 generates a vagal efferent output that counteracts inflammation mainly through
96 acetylcholine-induced inhibition of cytokine production (Borovikova et al., 2000). The
97 importance of this cholinergic anti-inflammatory mechanism is beyond doubt since its
98 dysfunction is involved in the pathophysiology of several conditions (Bassi et al., 2017;
99 Chang et al., 2019; Kanashiro et al., 2017; Li et al., 2011; van Maanen et al., 2009).
100 However, several studies have shown convincing evidence for the existence of other
101 neural mechanisms that regulate inflammation. For instance, animal and human
102 studies have demonstrated that the efferent sympathetic nervous system can
103 modulate inflammatory conditions through catecholamine-mediated suppression of
104 innate immune responses (Abe et al., 2017; Kox et al., 2014; Lankadeva et al., 2020;

105 Martelli et al., 2014; Tanaka et al., 2021; van Westerloo et al., 2011). Moreover, some
106 studies demonstrated that the sympathetic-mediated anti-inflammatory reflexes do not
107 depend on vagal afferent signalling, suggesting the existence of other peripheral
108 mechanisms able to detect inflammation and communicate with the central nervous
109 system to activate downstream sympathetic anti-inflammatory pathways (Abe et al.,
110 2017; Martelli et al., 2014).

111 In this regard, the carotid body, classically known as the main peripheral
112 monitor of the O₂ levels in the blood, has been considered a polymodal sensor due to
113 its particular ability to detect diverse molecules present in the circulation, such as
114 glucose, sodium chloride, hormones, and also, inflammatory mediators (Allen, 1998;
115 da Silva et al., 2019; Jendzjowsky et al., 2018; Katayama, 2016; Kumar and
116 Prabhakar, 2012; Thompson et al., 2016). In the context of inflammation, several
117 pieces of evidence indicate that the carotid bodies might be involved in the intricate
118 interplay between the immune system and the sympathetic nervous system. First, the
119 carotid body expresses receptors for inflammatory mediators such as
120 lysophosphatidic acid (LPA) and pro-inflammatory cytokines such as IL-1 β , IL-6, and
121 tumor necrosis factor-alpha (TNF- α) (Fernández et al., 2008; Jendzjowsky et al., 2018;
122 Kumar and Prabhakar, 2012; Mkrтчian et al., 2012; Wang et al., 2002). Second, LPA
123 and pro-inflammatory cytokines stimulate the carotid body and increase the carotid
124 sinus nerve (CSN) afferent activity in isolated *in vitro* preparations (Jendzjowsky et al.,
125 2021, 2018). Third, carotid body stimulation by its typical stimulus (hypoxia) activates
126 central autonomic areas that control parasympathetic (Erickson and Millhorn, 1994;
127 Zera et al., 2019) and, also, the sympathetic nervous system (Kline et al., 2010;
128 Koshiya and Guyenet, 1996; Luise King et al., 2012) which, besides vagally-mediated
129 mechanisms, represents an important component in the neural regulation of immunity
130 (Abe et al., 2017; Lankadeva et al., 2020; Martelli et al., 2014). Last, carotid body
131 denervation worsens systemic inflammation and accelerates multiple organ
132 dysfunction and death in rats with lipopolysaccharide (LPS)-induced sepsis (Nardocci
133 et al., 2015), suggesting that the carotid body is a protective factor during acute
134 inflammatory conditions. Altogether, these observations led to the hypothesis that the
135 carotid body plays a role in neuroimmune interactions, but the exact mechanisms
136 underlying this cross-talk are largely unknown.

137 In this study, we focused on investigating the impact of TNF- α (a ubiquitous
138 cytokine that triggers inflammation)(Grieve et al., 2017) on the carotid body-mediated

139 activation of the sympathetic nervous system, as well as the relevance of this
140 interaction in the modulation of TNF- α -induced systemic inflammation. We revealed
141 that the carotid body expresses the TNF- α receptor type I (TNFR1) and detects
142 increased levels of TNF- α in peripheral circulation, transmitting this information to the
143 brain via CSN afferent inputs to commissural nucleus tractus solitarius (cNTS)
144 glutamatergic neurons that project to rostral ventrolateral medulla (RVLM) pre-
145 sympathetic neurons, resulting in activation of the sympathetic nervous system to
146 counteract the TNF- α -induced inflammation. We, therefore, propose the existence of
147 a physiological carotid body-mediated neuroimmune reflex that acutely controls
148 inflammation. The identification of this neuroimmune reflex provides potential
149 mechanistic insights into the pathophysiology of inflammation-mediated diseases as
150 well as into the development of novel therapeutic strategies to treat these conditions.

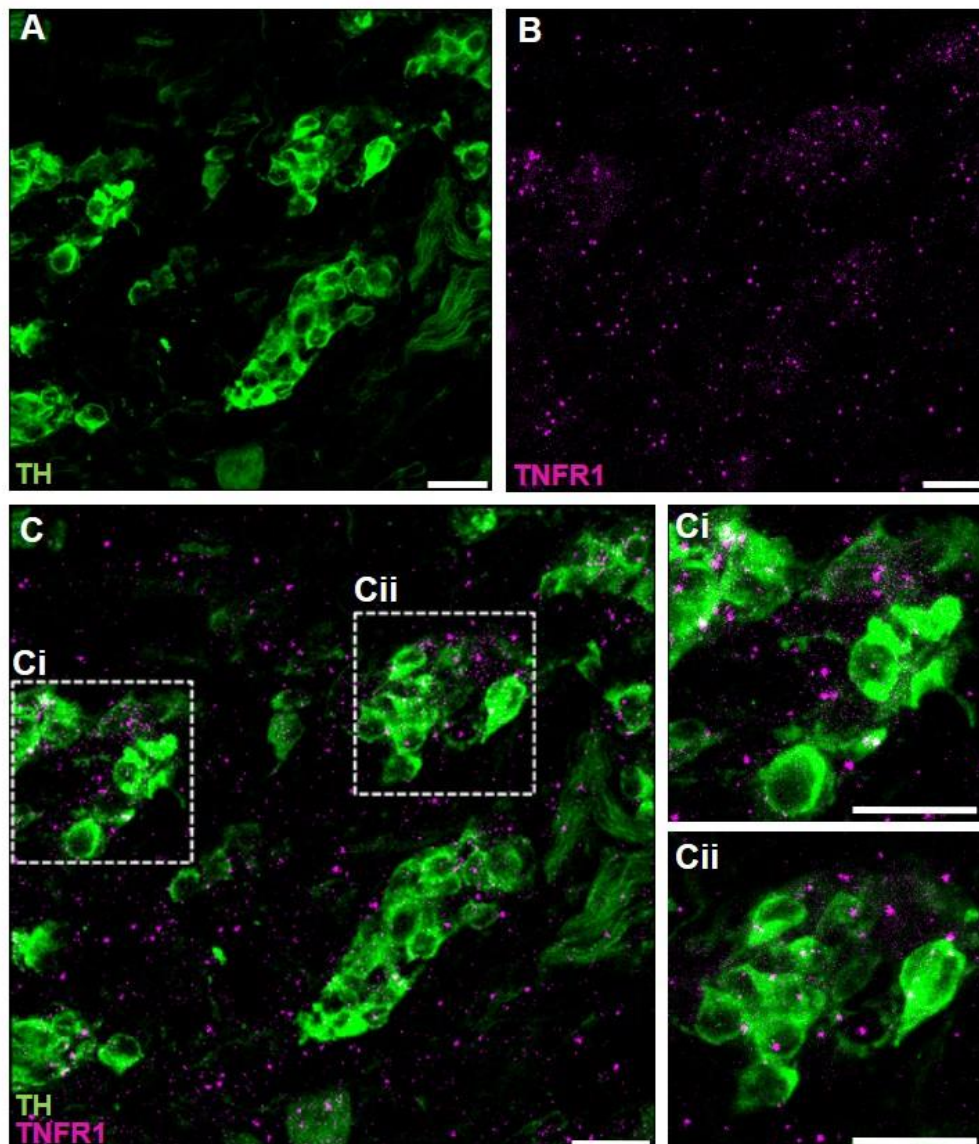
151
152
153
154
155
156
157
158
159
160
161
162
163
164
165
166
167
168
169
170
171
172

173 **Results**

174

175 **TNFR1 is expressed in the carotid body**

176 To verify the expression of TNF- α receptors type I (TNFR1) in the carotid body, we
177 used a combined approach of RNAscope *in situ* hybridization and
178 immunofluorescence. We found that the mRNA of TNFR1 is expressed in the carotid
179 body, characterized by clusters of tyrosine hydroxylase (TH)-positive cells (glomus
180 cells) (Fig. 1).



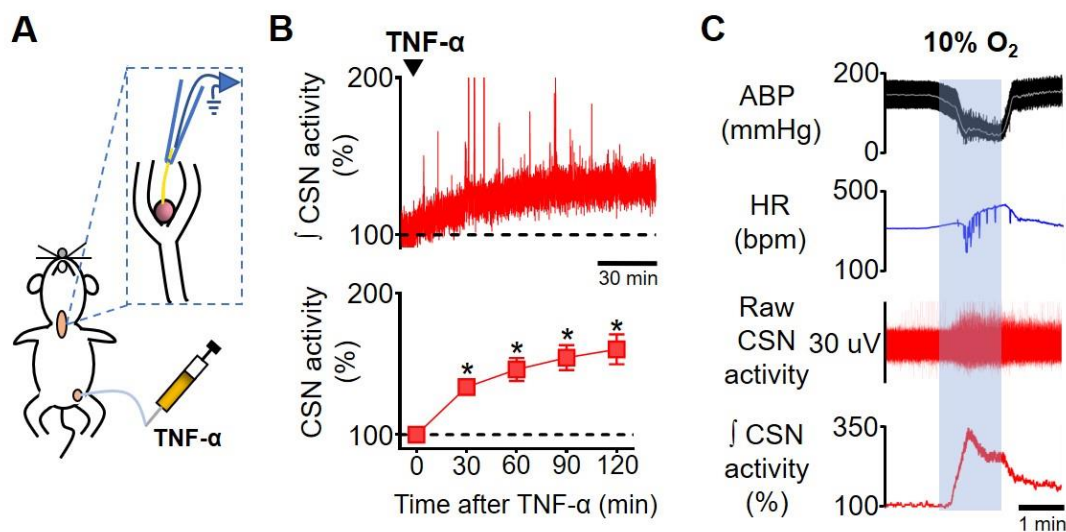
181

182 **Figure 1.** TNF- α receptors type I (TNFR1) are expressed in the carotid body of rats. Representative
183 section of a rat carotid body showing combined fluorescent *in situ* hybridization (TNFR1; magenta
184 puncta) and immunofluorescence (Tyrosine hydroxylase; TH; green staining). **A.** TH positive cells
185 (glomus cells) in the carotid body. **B.** RNAscope *in situ* hybridization showing TNFR1 mRNA expression
186 in the carotid body. **C.** Overlay of images a and b showing the colocalization of TH and TNFR1. **Ci** and
187 **Cii.** Zoom into selected regions of image C. Scale bars: 20 μ m.

188 **Circulating TNF- α increases carotid sinus nerve afferent activity**

189 Next, we investigated if elevated TNF- α levels in the blood could activate its receptors
190 in the carotid body and increase CSN activity in vivo. We found that exogenous TNF-
191 α administration increased CSN activity by $34 \pm 5\%$ at 30 minutes after administration
192 compared to baseline (Figure 2B). This TNF- α -induced excitation of CSN was
193 sustained and lasted the whole experiment ($46 \pm 7\%$, $55 \pm 8\%$, $60 \pm 10\%$ at 60, 90,
194 and 120 minutes after TNF- α administration, respectively; Figure 2B). Because
195 throughout the experimental protocol, the animals were artificially ventilated with a
196 slightly hyperoxia (50% O₂, balance N₂), it is very unlikely that the observed increase
197 in CSN activity was due a potential TNF- α -induced hypoxia. Our data suggest that the
198 carotid body could detect the circulating TNF- α and send signals to the central nervous
199 system through increases in CSN activity. We, therefore, hypothesized that the central
200 nervous system, in turn, might orchestrate complex autonomic responses, including
201 the activation of the sympathetic nervous system.

202



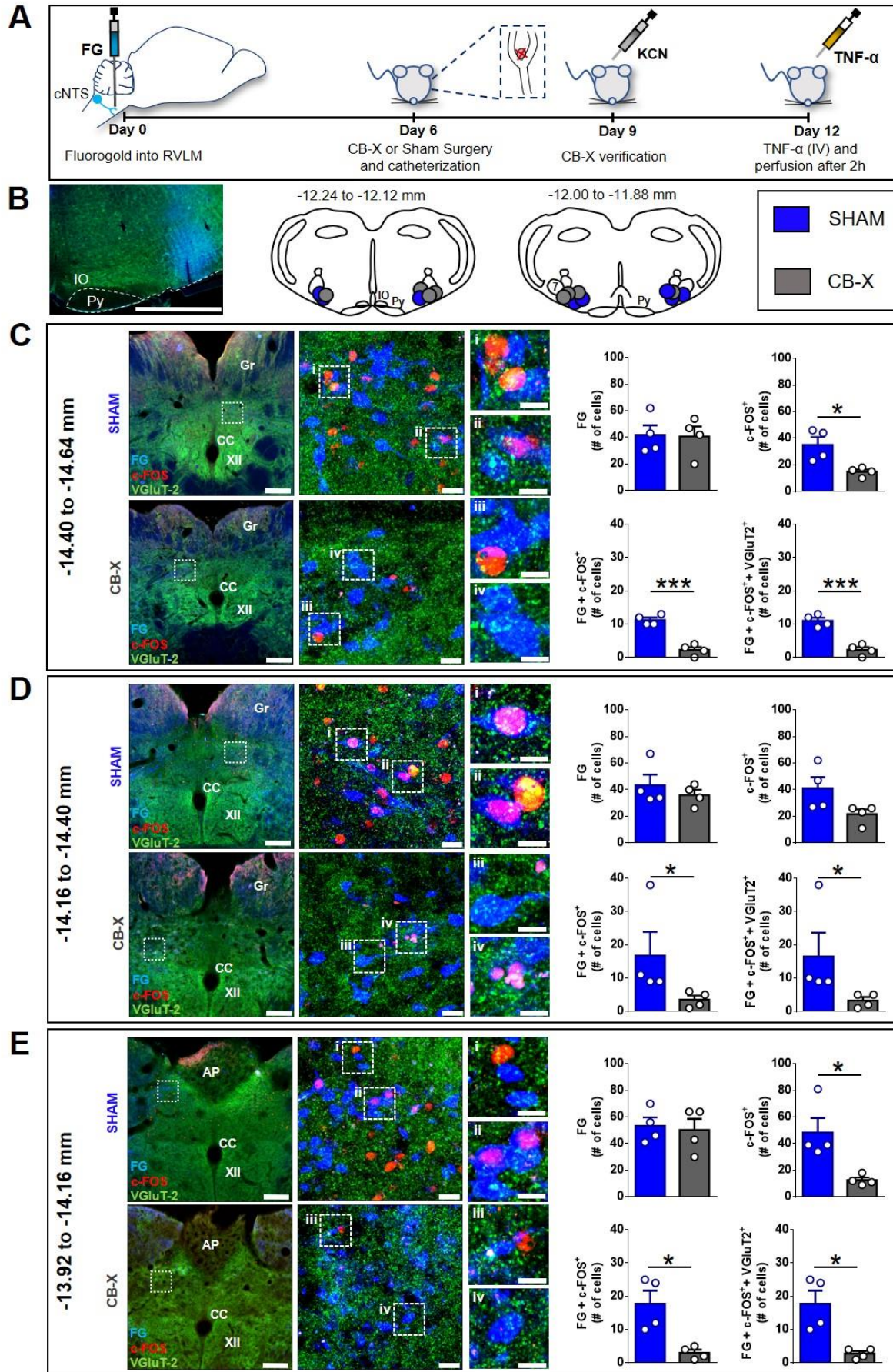
203

204 **Figure 2.** Carotid sinus nerve afferent activity (CSN activity) in response to intravenous TNF- α . **A.**
205 Schematic illustration of the experimental protocol. **B.** Representative trace of the integrated CSN
206 activity (\int CSN activity; time constant = 1 s) from one rat during baseline and after TNF- α (500 ng, IV,
207 black arrowhead) administration (top; scale bar = 30 minutes) and summary data showing CSN activity
208 at baseline and 30, 60, 90 and 120 minutes after TNF- α administration (bottom; n = 6). Baseline CSN
209 activity was normalized to 100% after noise subtraction. A one-way repeated measures ANOVA
210 detected statistically significant differences in CSN activity over time, $F_{(4, 20)} = 21,282$, $p < 0.001$.
211 Subsequent post hoc analysis with a Bonferroni adjustment revealed that, as compared to time 0
212 (baseline), CSN activity was statistically significantly higher at 30 minutes (34%, 95% CI [9, 59], $p =$
213 0.014); at 60 minutes (46%, 95% CI [8, 85], $p = 0.023$); at 90 minutes (55%, 95% CI [13, 96], $p = 0.016$);
214 and at 120 minutes (60%, 95% CI [10, 111], $p = 0.023$) after TNF- α administration. * $p < 0.05$. Data are
215 means \pm SEM. **C.** Representative traces showing the viability of CSN activity recordings assessed by
216 a brief exposure to hypoxia (10% O₂, balance N₂; grey shaded area). The typical acute response of
217 urethane-anesthetized rats to hypoxia includes hypotension, bradycardia, and a robust increase in CSN
218 activity. ABP, arterial blood pressure; HR, heart rate.

219 **RVLM-projecting cNTS glutamatergic neurons are activated by TNF- α**

220 The first synapse of carotid body afferents within the central nervous system occurs in
221 the cNTS, as extensively described in the literature (Colombari et al., 1996; Cruz et
222 al., 2010; Kline et al., 2010; Malheiros-Lima et al., 2020). The cNTS sends excitatory
223 glutamatergic projections to several areas, being implicated in diverse physiological
224 functions. In the context of the carotid body-related functions, the cNTS neurons
225 project to important autonomic areas involved in the neural control of cardiovascular
226 and respiratory functions (Kline et al., 2010; Zera et al., 2019). For example, a previous
227 report demonstrated direct monosynaptic projections from cNTS to RVLM, where the
228 majority of pre-sympathetic neurons are located (Kline et al., 2010). It was also shown
229 that most of these RVLM-projecting cNTS neurons are activated by hypoxia and
230 constitute the major neural pathway of hypoxia-induced sympathetic activation (Kline
231 et al., 2010; Koshiya and Guyenet, 1996). Thus, we sought to investigate if this
232 sympathoexcitatory pathway is activated by circulating TNF- α since this cytokine
233 increased the discharge of carotid body afferents, as shown in Figure 2B. Our results
234 demonstrated massive monosynaptic projections from cNTS to RVLM (FG-labeled
235 cells, blue staining, Figure 3C – E) in both SHAM and CB-X rats at all evaluated rostro-
236 caudal levels: -14.40 mm to -14.64 mm (SHAM, 42 ± 7 cells; CB-X, 41 ± 7 cells), -
237 14.16 mm to -14.40 mm (SHAM, 43 ± 8 cells; CB-X, 36 ± 4 cells), and -13.92 mm to -
238 14.16 mm. (SHAM, 53 ± 6 cells; CB-X, 50 ± 8 cells). Most of these projections are
239 excitatory (VGLuT2⁺ cells, green staining, Figure 3C – E). Circulating TNF- α activated
240 a considerable proportion of these RVLM-projecting glutamatergic cNTS neurons in
241 SHAM rats, as indicated by c-FOS expression (red staining) in FG⁺/VGLuT2⁺ cells
242 (Figure 3C – E); Importantly, the number of activated RVLM-projecting glutamatergic
243 cNTS neurons was dramatically reduced by carotid body ablation: -14.40 mm to -14.64
244 mm (SHAM, 11 ± 1 cells; CB-X, 2 ± 1 cells), -14.16 mm to -14.40 mm (SHAM, 17 ± 7
245 cells; CB-X, 3 ± 1 cells), and -13.92 mm to -14.16 mm. (SHAM, 18 ± 4 cells; CB-X, 3
246 ± 1 cells). The efficacy of the bilateral carotid body ablation procedure was confirmed
247 by the lack of cardiovascular responses to KCN (figure supplement 1A – B). Together
248 with our previous findings (Figures 1 and 2), these results suggest that the carotid
249 body detects the circulating TNF- α through TNFR1 and transmits this information to
250 the central nervous system via carotid sinus nerve afferents, resulting in the activation
251 of a sympathoexcitatory pathway.

252



255 **Figure 3.** Activation of RVLM-projecting cNTS glutamatergic neurons by circulating TNF- α in SHAM
256 and CB-X rats. **A.** Schematic illustration of the experimental protocol. **B.** Representative image from a
257 typical retrograde tracer (Fluorogold; FG) injection-site into RVLM and schematic pictures of RVLM
258 injections-sites of all bilaterally FG-injected animals (n=4 per group). IO, inferior olive; Py, pyramidal
259 tract; 7, facial motor nucleus. Scale bar is 1000 μ m. **C, D** and **E.** Images are representative pictures of
260 cNTS sections at three different rostro-caudal levels, processed for c-FOS (red) and VGluT2 (green)
261 immunofluorescence, and containing FG-positive cells retrogradely labeled from the RVLM (blue). Gr,
262 gracile nucleus; CC, central canal; XII, hypoglossal nucleus; AP, area postrema. Scale bars are 200
263 μ m for 5x magnification pictures (left), 20 μ m for 40x magnification pictures (middle) and 10 μ m for
264 zoom pictures (right). **i, ii, iii,** and **iv.** Digital zoom into selected regions. Bar graphs show the
265 quantification of retrogradely labeled FG neurons, c-FOS⁺ neurons, double stained (FG/c-FOS⁺)
266 neurons and triple stained (FG/c-FOS⁺/VGluT2⁺) neurons in the cNTS 2 hours after TNF- α
267 administration (500 ng, IV) in SHAM (n=4) and CB-X (n=4) rats. The number of RVLM-projecting
268 neurons (FG-labeled cells) was not different between SHAM and CB-X rats in all evaluated cNTS levels:
269 -14.40 to -14.64 mm (C), $t(6) = 0.096$, $p = 0.926$ (Student's t -test); -14.16 to -14.40 mm (D), $U = 7.5$, z
270 $= -0.145$, $p = 0.886$ (Mann-Whitney U -test); and -13.92 to -14.16 mm (E), $t(6) = 0.285$, $p = 0.785$
271 (Student's t -test). General neuronal activation (i.e., both RVLM-projecting and RVLM- non-projecting;
272 c-FOS⁺ cells) was higher in SHAM as compared to CB-X rats at -14.40 to -14.64 mm (C), $t(3.505) =$
273 3.326 , $p = 0.036$ (Welch's t -test) and at -13.92 to -14.16 mm (E), $U = 0$, $z = -2.323$, $p = 0.029$ (Mann-
274 Whitney U -test); but not at -14.16 to -14.40 mm (D), $t(6) = 2.141$, $p = 0.076$ (Student's t -test). The
275 specific activation of RVLM-projecting neurons (c-FOS⁺/FG⁺ cells) was higher in SHAM as compared to
276 CB-X rats in all 3 cNTS levels: -14.40 to -14.64 mm (C), $t(6) = 7.919$, $p < 0.001$ (Student's t -test); -14.16
277 to -14.40 mm (D), $U = 0$, $z = -2.323$, $p = 0.029$ (Mann-Whitney U -test); and -13.92 to -14.16 mm (E),
278 $t(3.324) = 3.661$, $p = 0.030$ (Welch's t -test). Virtually all activated RVLM-projecting cNTS neurons are
279 glutamatergic (FOS⁺/FG/VGluT2⁺ cells). The number of activated RVLM-projecting cNTS glutamatergic
280 neurons was higher in SHAM as compared to CB-X rats in all 3 cNTS levels: -14.40 to -14.64 mm (C),
281 $t(6) = 7.000$, $p < 0.001$ (Student's t -test); -14.16 to -14.40 mm (D), $U = 0$, $z = -2.337$, $p = 0.029$ (Mann-
282 Whitney U -test); and -13.92 to -14.16 mm (E), $t(3.219) = 3.755$, $p = 0.029$ (Welch's t -test). * $p < 0.05$
283 and *** $p < 0.001$. Data are means \pm SEM.

284

285

286

287

288

289

290

291

292

293

294

295

296

297

298

299

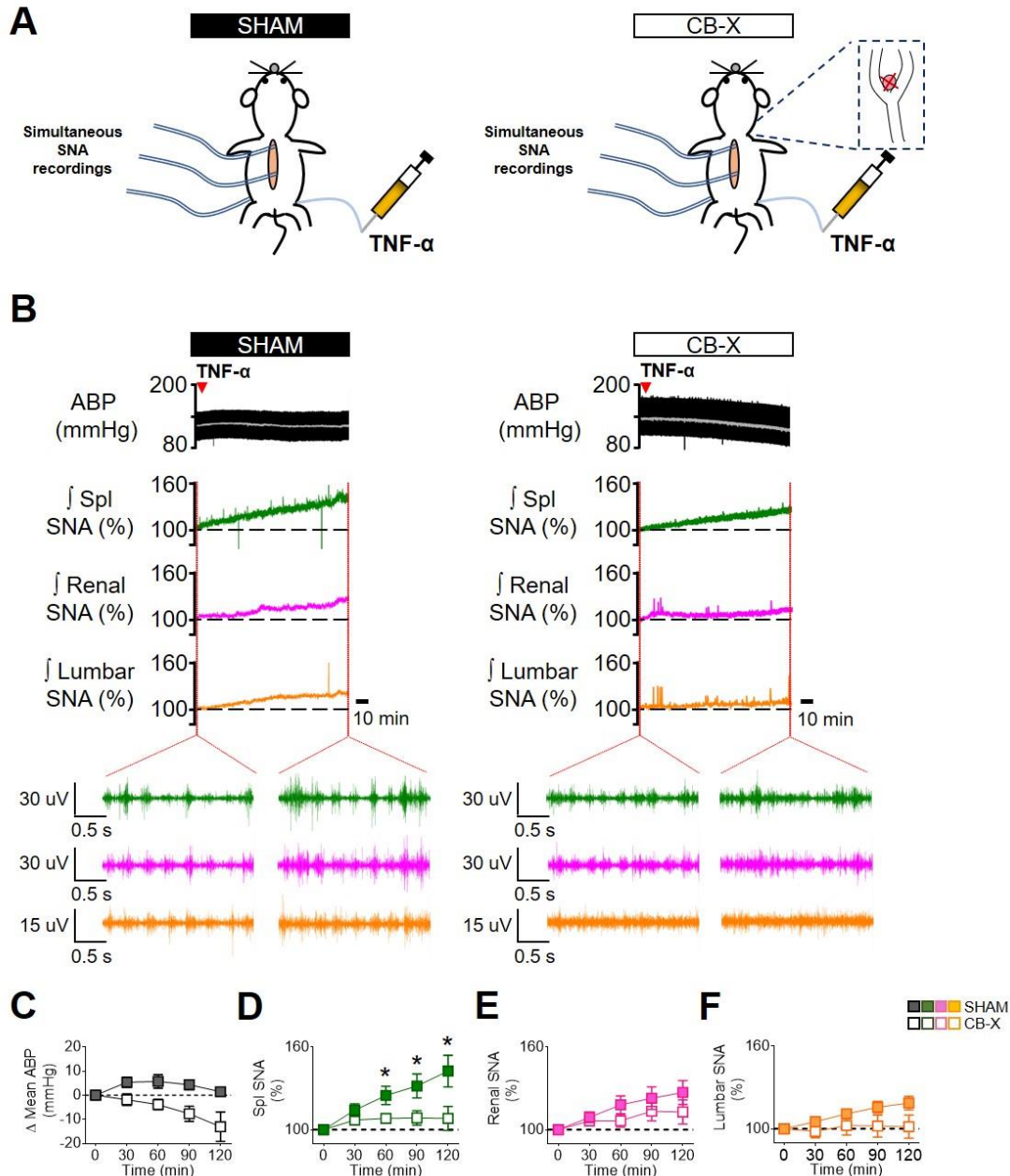
300

301 **TNF- α promotes a carotid-body mediated increase in splanchnic SNA**

302 Because circulating TNF- α activated a well-known sympathoexcitatory central
303 pathway, we next performed experiments to investigate the effect of this cytokine on
304 sympathetic activity directly recorded from multiple sympathetic nerves in vivo. Our
305 results showed that intravenously administered TNF- α promotes a generalized
306 sympathoexcitation in SHAM rats (Figure 4B – F), consistent with the activation of the
307 RVLN-projecting cNTS glutamatergic neurons demonstrated in Figure 3: Δ Splanchnic
308 SNA ($14 \pm 4\%$, $25 \pm 7\%$, $32 \pm 9\%$ and $42 \pm 11\%$ respectively at 30, 60, 90, and 120
309 minutes after TNF- α administration); Δ Renal SNA ($9 \pm 4\%$, $18 \pm 6\%$, $22 \pm 8\%$, $27 \pm$
310 9% respectively at 30, 60, 90, and 120 minutes after TNF- α administration) and Δ
311 lumbar SNA ($5 \pm 1\%$, $11 \pm 3\%$, $16 \pm 4\%$, $19 \pm 5\%$ respectively at 30, 60, 90, and 120
312 minutes after TNF- α administration). Interestingly, despite the generalized
313 sympathetic activation, mean arterial blood pressure (ABP) only slightly increased
314 (Figure 4B – C).

315 Since carotid body ablation almost abolished the TNF- α -induced activation of
316 RLVM-projecting cNTS glutamatergic neurons (Figure 3), we tested whether the
317 carotid bodies would be necessary to the observed sympathoexcitation in response to
318 TNF- α administration. To accomplish that, we administered TNF- α to rats subjected to
319 bilateral carotid body ablation (Figure 4B – F). CB-X rats displayed an attenuated
320 increase in SNA in response to TNF- α : Δ Splanchnic SNA ($7 \pm 1\%$, $8 \pm 2\%$, $8 \pm 5\%$
321 and $8 \pm 9\%$ respectively at 30, 60, 90, and 120 minutes after TNF- α administration), Δ
322 renal SNA ($6 \pm 3\%$, $6 \pm 5\%$, $13 \pm 7\%$ and $13 \pm 9\%$ respectively at 30, 60, 90, and 120
323 minutes after TNF- α administration), and Δ lumbar SNA ($-2 \pm 5\%$, $2 \pm 7\%$, $2 \pm 8\%$ and
324 $1 \pm 8\%$ respectively at 30, 60, 90, and 120 minutes after TNF- α administration). These
325 SNA responses were diminished compared to those displayed by SHAM rats,
326 especially on splanchnic SNA at 60, 90, and 120 minutes after TNF- α administration,
327 suggesting that the carotid bodies contribute to this specific response (Figure 4D).
328 Unlike SHAM rats, mean ABP in CB-X rats tended to decrease even without
329 reductions in the activity of any of the recorded sympathetic nerves (Figure 4B – C).
330 At the end of the experiments, bilateral carotid body ablation was confirmed by the
331 lack of sympathetic and blood pressure responses to KCN (figure supplement 2A –
332 B).

333



334

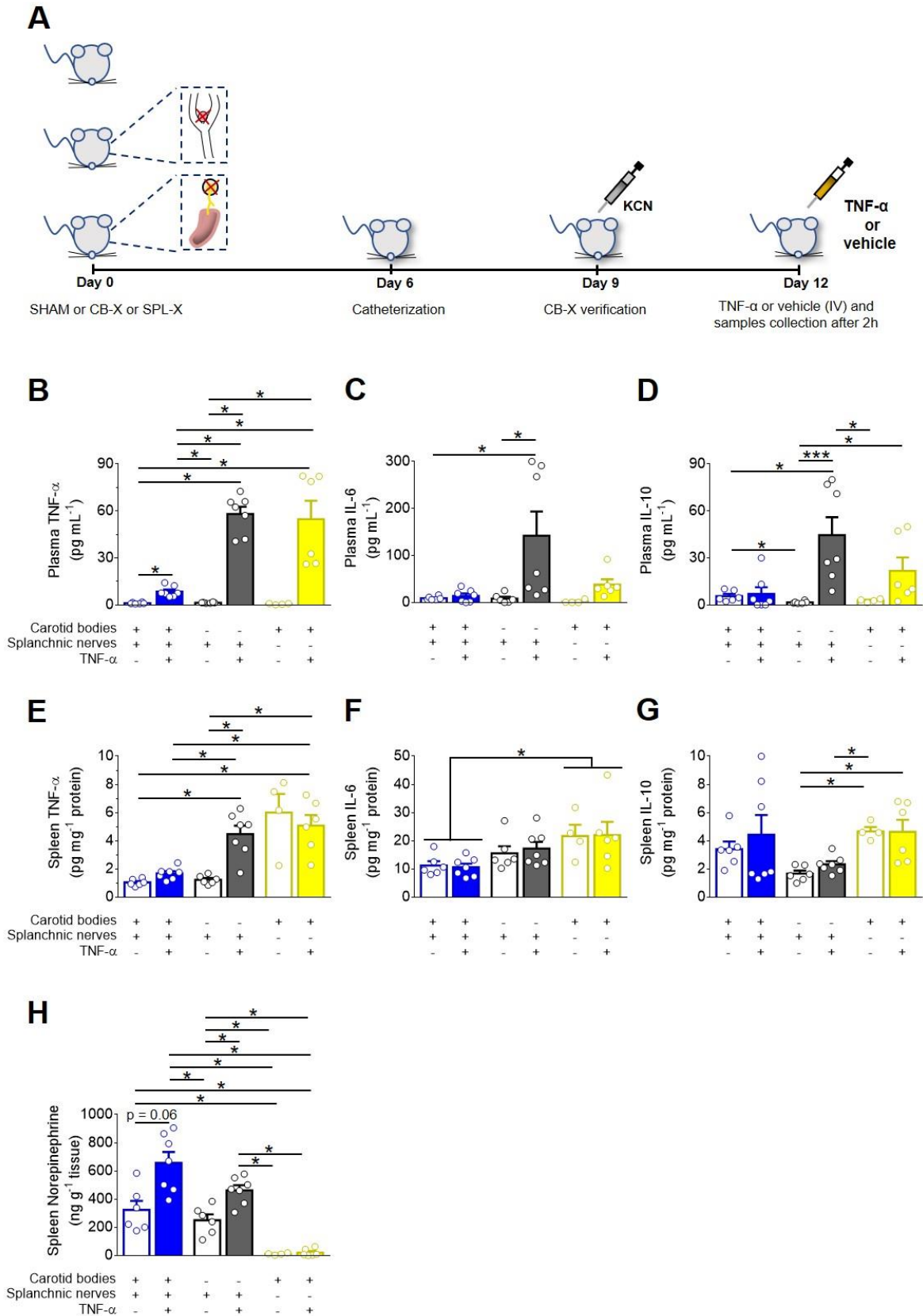
335 **Figure 4.** Carotid body ablation attenuates the TNF- α -induced splanchnic sympathetic activation. **A.**
 336 Schematic illustration of the experimental protocol. **B.** Representative traces of arterial blood pressure
 337 (pulsatile ABP, black; mean ABP, white), splanchnic (Spl; green), renal (magenta) and lumbar (orange)
 338 integrated (\int ; time constant = 1s) sympathetic nerve activity (SNA) in sham-operated rats (SHAM) and
 339 carotid body-ablated rats (CB-X) during baseline conditions and in the next 2 hours after TNF- α
 340 administration (500 ng, IV, red arrowhead). For each sympathetic nerve, raw SNA signals at baseline
 341 and 2 hours after TNF- α administration are also presented (as indicated by the red dotted lines). **C, D,**
 342 **E and F.** Summary data showing the changes in mean ABP (**C**), Spl SNA (**D**), Renal SNA (**E**)
 343 and Lumbar SNA (**F**) in response to TNF- α in SHAM (filled symbols, n = 6) and CB-X (open symbols, n = 6)
 344 rats. For each rat, baseline integrated SNA was normalized to 100%, and the relative changes were
 345 calculated at four different time points (30, 60, 90 and 120 minutes after TNF- α administration). A
 346 statistically significant group x time interaction on spl SNA was detected by two-way repeated-measures
 347 ANOVA, $F_{(3,15)} = 11.119$, $p < 0.001$. Subsequent simple main effects analyses revealed that spl SNA
 348 changes were significantly greater in SHAM as compared to CB-X rats at 60 minutes, $F_{(1,5)} = 7.042$, p
 349 $= 0.045$; at 90 minutes, $F_{(1,5)} = 10.224$, $p = 0.024$; and at 120 minutes, $F_{(1,5)} = 16.515$, $p = 0.010$ after
 350 TNF- α administration. * $p < 0.05$. There were no statistically significant group x time interactions on
 351 Mean ABP, $F_{(3,15)} = 0.807$, $p = 0.420$, $\epsilon = 0.371$; Renal SNA, $F_{(3,15)} = 0.805$, $p = 0.510$; and Lumbar
 352 SNA, $F_{(3,15)} = 1.685$, $p = 0.213$ (two-way repeated measures ANOVA). Data are means \pm SEM.

353 **Carotid body ablation or splanchnic sympathetic denervation exacerbates TNF-**
354 **α -induced inflammation**

355 Considering that the exogenous TNF- α activated a carotid body-cNTS-RVLM circuitry
356 to excite a specific sympathetic nerve (splanchnic), and because the splanchnic
357 sympathetic nerves have been considered essential components of sympathetic-
358 mediated mechanisms to control inflammation (Lankadeva et al., 2020; Martelli et al.,
359 2014), we next investigated if the activation of this newly described circuit could play
360 an anti-inflammatory role in the TNF- α -induced inflammation. We found that, in SHAM
361 rats that received TNF- α , the plasma levels of this cytokine (8.5 ± 1.3 pg mL⁻¹) were
362 found significantly higher in comparison to SHAM rats that received vehicle (1.1 ± 0.2
363 pg mL⁻¹) (Figure 5B). It is important to mention that, the half-life of TNF- α is very short
364 (few minutes) (Ma et al., 2015; Simó et al., 2012), and, hence, it is very likely that the
365 measured levels of this cytokine in the plasma (2 hours after TNF- α or vehicle
366 administrations) reflect endogenously produced TNF- α . In rats subjected to either
367 carotid body ablation (CB-X) or splanchnic sympathetic denervation (SPL-X), the
368 administration of TNF- α resulted in significant higher plasma levels of this cytokine
369 compared to SHAM rats injected with TNF- α (CB-X + TNF- α = 58.1 ± 4.7 pg mL⁻¹,
370 SPL-X + TNF- α = 54.8 ± 11.8 pg mL⁻¹) (Figure 5B), suggesting that the absence of the
371 carotid bodies or the splanchnic sympathetic nerves exacerbated the systemic
372 inflammatory status triggered by the exogenous TNF- α . In the same direction, the
373 levels of TNF- α in the spleen were found higher in CB-X + TNF- α (4.5 ± 0.6 pg mg⁻¹)
374 and in SPL-X + TNF- α (5.1 ± 0.8 pg mg⁻¹) groups compared to SHAM + TNF- α ($1.7 \pm$
375 0.2 pg mg⁻¹) group (Figure 5E). These results support the idea that the exogenously
376 administered TNF- α induced the endogenous production of additional TNF- α likely via
377 stimulation of splenic macrophages and, that, the removal of the carotid bodies (a
378 potential sensor of TNF- α) or of the splanchnic sympathetic nerves (a potential
379 suppressor of spleen-derived TNF- α production), significantly increased TNF- α levels
380 in the spleen. It is important to highlight that in SPL-X + vehicle animals, the levels of
381 TNF- α in the spleen were also elevated (6.0 ± 1.3 pg mg⁻¹) (Figure 5E), reinforcing the
382 notion that the splanchnic sympathetic innervation of the spleen (via celiac ganglion),
383 exerts a kind of inhibitory tonus over splenic production of TNF- α . By way of
384 comparison, in rats with intact splanchnic nerves (SHAM and CB-X) injected with
385 vehicle, the levels of TNF- α in the spleen were low: (SHAM + vehicle = 1.0 ± 0.1 pg
386 mg⁻¹, CB-X + vehicle = 1.2 ± 0.1 pg mg⁻¹) (Figure 5E).

387 Regarding plasma IL-6 levels, CB-X + TNF- α animals displayed higher levels
388 (142.2 \pm 51.0 pg mL⁻¹) than SHAM + vehicle (9.1 \pm 1.6 pg mL⁻¹) and CB-X + vehicle
389 (8.2 \pm 3.8 pg mL⁻¹) (Figure 5C). Although not statistically significant, the levels of IL-6
390 in the plasma tended to be higher in CB-X + TNF- α and SPL-X + TNF- α (38.1 \pm 11.2
391 pg mL⁻¹) compared to all other groups: (SHAM + vehicle = 9.1 \pm 1.6 pg mL⁻¹, SHAM +
392 TNF- α = 14.1 \pm 5.0 pg mL⁻¹, CB-X + vehicle = 8.2 \pm 3.8 pg mL⁻¹, SPL-X + vehicle =
393 2.2 \pm 1.9 pg mL⁻¹) (Figure 5C). Concerning the spleen levels of IL-6, no interactions
394 between group x treatment were detected by two-way ANOVA. However, a statistically
395 main effect of group indicated that the spleen levels of IL-6 were higher in SPL-X +
396 vehicle (21.7 \pm 4.0 pg mg⁻¹) and SPL-X + TNF- α (22.0 \pm 4.7 pg mg⁻¹) groups compared
397 to SHAM + vehicle (11.2 \pm 1.5 pg mg⁻¹) and SHAM + TNF- α (10.6 \pm 1.3 pg mg⁻¹)
398 groups (Figure 5F), suggesting that splanchnic sympathetic denervation was
399 permissive to IL-6 production in the spleen, even in the absence of the TNF- α stimulus.
400 With regard to plasma IL-10, the levels of this anti-inflammatory cytokine tended to be
401 higher in CB-X + TNF- α (44.7 \pm 11.4 pg mL⁻¹) and SPL-X + TNF- α (21.7 \pm 8.6 pg mL⁻¹)
402 ¹) as compared to SHAM + TNF- α (7.1 \pm 4.2 pg mL⁻¹) and to every other group that
403 received vehicle (SHAM + vehicle = 5.6 \pm 1.4 pg mL⁻¹, CB-X + vehicle = 1.7 \pm 0.3 pg
404 mL⁻¹, SPL-X + vehicle = 2.8 \pm 0.5 pg mL⁻¹) (Figure 5D). These results match with the
405 increased levels of TNF- α in the plasma and the spleen of CB-X and SPL-X rats that
406 received TNF- α , indicating a worse systemic inflammatory status in these animals.
407 Finally, spleen levels of IL-10 tended to be lower in both CB-X groups, but was only
408 statistically different between: CB-X + vehicle (1.7 \pm 0.2 pg mg⁻¹) compared to SPL-X
409 + vehicle (4.7 \pm 0.3 pg mg⁻¹); CB-X + vehicle group compared to SPL-X + TNF- α (4.6
410 \pm 0.9 pg mg⁻¹); and between CB-X + TNF- α (2.3 \pm 0.2 pg mg⁻¹) compared to SPL-X +
411 vehicle (Figure 5G). In regard to norepinephrine levels in the spleen, SHAM rats
412 injected with TNF- α displayed the highest mean levels (656.2 \pm 77.6 pg mg⁻¹), followed
413 by CB-X + TNF- α (462.3 \pm 36.4 pg mg⁻¹), SHAM + vehicle (322.9 \pm 64.4 pg mg⁻¹), CB-
414 X+ vehicle (249.9 \pm 40.9 pg mg⁻¹), SPL-X + TNF- α (20.6 \pm 10.7 pg mg⁻¹), and SPL-X
415 + vehicle (10.3 \pm 3.5 pg mg⁻¹) groups (Figure 5H). Note that splanchnic sympathetic
416 denervation almost depleted the norepinephrine content in the spleen, confirming the
417 efficacy of the denervation procedure. In addition, the efficacy of splanchnic
418 sympathetic denervation was also verified by the less pronounced TH staining in the
419 spleen (figure supplement 3C). The efficacy of the bilateral carotid body ablation
420 procedure was confirmed by the lack of cardiovascular responses to KCN (figure

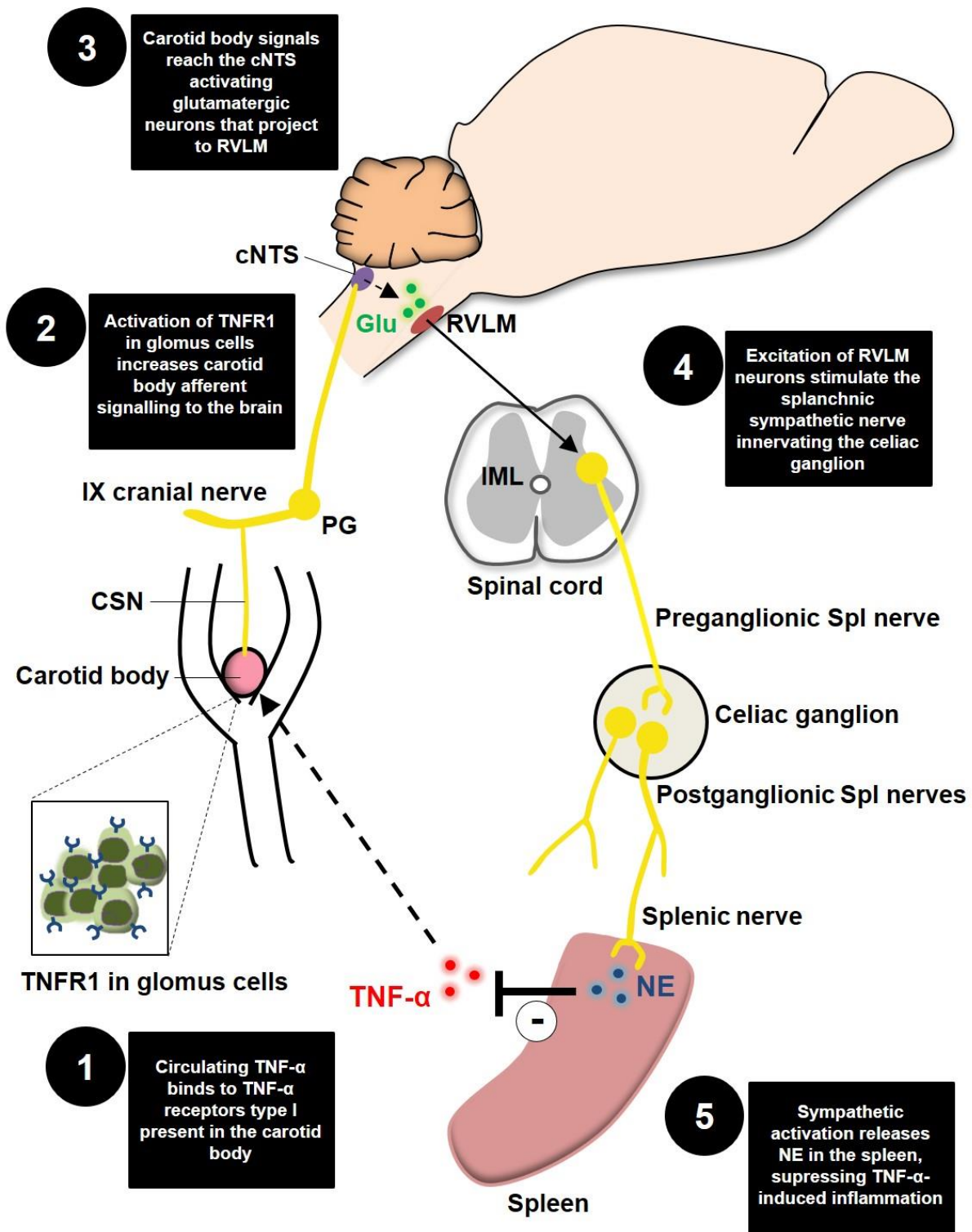
421 supplement 3A – B). Collectively, our data suggest that elevated circulating levels of
422 TNF- α activates a neural mechanism (carotid body-cNTS-RVLM-splanchnic
423 sympathetic nerves) that controls the ongoing inflammation by inhibiting the synthesis
424 of additional TNF- α in the spleen likely via direct norepinephrine-mediated
425 suppression of splenic macrophage TNF- α production.



426

427 **Figure 5.** Carotid body ablation (CB-X) or splanchnic sympathetic denervation (SPL-X) intensify the
 428 TNF- α -induced inflammation. **A.** Schematic illustration of the experimental protocol. **B, C and D.**
 429 Plasma levels of TNF- α , IL-6 and IL-10 in SHAM (blue bars), CB-X (gray bars), and SPL-X (yellow bars)
 430 rats, measured 2 hours after vehicle (empty bars) or TNF- α (filled bars) intravenous administration (n =
 431 4 - 7 per group). **B.** Statistically significant differences in the plasma levels of TNF- α across groups were

432 detected: $H(5) = 31.454$, $p < 0.001$ (Kruskal-Wallis). In SHAM + TNF- α , the plasma levels of this cytokine
433 were found significantly higher in comparison to SHAM + vehicle ($U = 0$, $z = -3.000$, $p = 0.001$, Mann-
434 Whitney U -test). In CB-X and SPL-X rats, TNF- α administration resulted in significant higher plasma
435 levels of this cytokine as compared to SHAM + TNF- α : SHAM + TNF- α vs. CB-X + TNF- α ($U = 0$, $z = -$
436 3.130 , $p = 0.001$, Mann-Whitney U -test); SHAM + TNF- α vs. SPL-X + TNF- α ($U = 0$, $z = -3.000$, $p =$
437 0.001 , Mann-Whitney U -test). Between vehicle-treated groups, the plasma levels of TNF- α were not
438 different ($p > 0.003$). Regarding plasma IL-6 levels, significant differences between groups were
439 detected: $H(5) = 22.024$, $p = 0.001$ (Kruskal-Wallis). **C.** The plasma levels of IL-6 were higher in CB-X
440 + TNF- α as compared to SHAM + vehicle ($U = 1$, $z = -2.857$, $p = 0.002$, Mann-Whitney U -test) and to
441 CB-X + vehicle ($U = 1$, $z = -2.857$, $p = 0.002$, Mann-Whitney U -test). No statistical differences were
442 found in plasma levels of IL-6 in the other pairwise comparisons ($p > 0.003$). **D.** Finally, the plasma
443 levels of IL-10 were found significantly different across groups: $F_{(5, 13.522)} = 14.524$, $p < 0.001$ (Welch
444 ANOVA). Games-Howell post hoc test revealed that the plasma levels of IL-10 were significantly higher
445 in CB-X + TNF- α as compared to all groups that received vehicle: CB-X + TNF- α vs. SHAM + vehicle
446 (Mean difference = 2.0 pg mL^{-1} , 95% CI [0.6, 3.3], $p = 0.005$); CB-X + TNF- α vs. CB-X + vehicle (Mean
447 difference = 3.1 pg mL^{-1} , 95% CI [1.8, 4.4], $p < 0.001$); CB-X + TNF- α vs. SPL-X + vehicle (Mean
448 difference = 2.6 pg mL^{-1} , 95% CI [1.2, 3.9], $p = 0.001$). In SPL-X + TNF- α , the plasma levels of IL-10
449 were higher as compared to CB-X + vehicle (Mean difference = 2.2 pg mL^{-1} , 95% CI [0.2, 4.1], $p =$
450 0.032). Between vehicle-administered groups, SHAM rats displayed higher plasma levels of IL10 as
451 compared to CB-X rats (Mean difference = 1.2 pg mL^{-1} , 95% CI [0.1, 2.2], $p = 0.033$). **E, F and G.** Spleen
452 levels of TNF- α , IL-6 and IL-10 in SHAM (blue bars), CB-X (gray bars), and SPL-X (yellow bars) rats, 2
453 hours after vehicle (empty bars) or TNF- α (filled bars) intravenous administration ($n = 4 - 7$ per group).
454 **E.** Statistically significant differences in the spleen levels of TNF- α between groups were found: $F_{(5,$
455 $12.262)} = 12.957$, $p < 0.001$ (Welch ANOVA). Games-Howell post hoc test revealed that the spleen levels
456 of TNF- α were significantly higher in CB-X and SPL-X that received TNF- α as compared to SHAM rats
457 that received TNF- α : CB-X + TNF- α vs. SHAM + TNF- α (Mean difference = 2.8 pg mg^{-1} protein, 95%
458 CI [0.5, 5.1], $p = 0.021$); SPL-X + TNF- α vs. SHAM + TNF- α (Mean difference = 3.4 pg mg^{-1} protein,
459 95% CI [0.2, 6.6], $p = 0.039$). Within vehicle-treated groups, the spleen levels of TNF- α were not different
460 ($p > 0.05$). No statistical differences were found when comparing SHAM + vehicle vs. SHAM + TNF- α
461 (Mean difference = -0.6 pg mg^{-1} protein, 95% CI [-1.3, 0.0], $p = 0.064$). **F.** Regarding the spleen levels
462 of IL-6, no interactions between group x treatment were detected: $F_{(2,30)} = 0.092$, $p = 0.912$, partial $\eta^2 =$
463 0.006 . However, a statistically significant main effect of group was found: $F_{(2,30)} = 7.130$, $p = 0.003$,
464 partial $\eta^2 = 0.322$. A Bonferroni post hoc analysis indicated that the spleen levels of IL-6 were significant
465 higher in SPL-X groups as compared to SHAM groups: (Mean difference = $10.9 \text{ pg mg protein}$, 95% CI
466 [3.5, 18.3], $p = 0.002$). **G.** Concerning the spleen levels of IL-10, statistically significant differences
467 between groups were found: $F_{(5, 13.792)} = 12.491$, $p < 0.001$ (Welch ANOVA). Games-Howell post hoc
468 test revealed that the spleen levels of IL-10 were significantly lower in CB-X groups as compared to
469 SPL-X groups: CB-X + vehicle vs. SPL-X + vehicle (Mean difference = -1.1 pg mg^{-1} protein, 95% CI [-
470 $1.6, -0.5$], $p = 0.002$); CB-X + vehicle vs. SPL-X + TNF- α (Mean difference = -1.0 pg mg^{-1} protein, 95%
471 CI [-1.8, -0.1], $p = 0.026$); CB-X + TNF- α vs. SPL-X + vehicle (Mean difference = -0.7 pg mg^{-1} protein,
472 95% CI [-1.1, -0.3], $p = 0.002$). **H.** Spleen levels of norepinephrine in SHAM (blue bars), CB-X (gray
473 bars), and SPL-X (yellow bars) rats, 2 hours after vehicle (empty bars) or TNF- α (filled bars) intravenous
474 administration ($n = 4 - 7$ per group).. Statistically significant differences in the spleen levels of
475 norepinephrine between groups were found: $F_{(5, 13.050)} = 45.864$, $p < 0.001$ (Welch ANOVA). * $p < 0.05$
476 and *** $p < 0.001$. Data are means \pm SEM. Games-Howell post hoc test revealed that the administration
477 of TNF- α in SHAM rats, resulted in a trend to increase the spleen norepinephrine levels compared to
478 SHAM animals receiving vehicle (Mean difference = 333.3 pg mg^{-1} tissue, 95% CI [-11.2, 677.8], $p =$
479 0.060) and in significant increases as compared to CB-X + vehicle (Mean difference = 406.3 pg mg^{-1}
480 tissue, 95% CI [94.4, 718.2], $p = 0.011$), to SPL-X + vehicle (Mean difference = 645.9 pg mg^{-1} tissue,
481 95% CI [337.1, 954.7], $p = 0.001$), and to SPL-X + TNF- α (Mean difference = 635.5 pg mg^{-1} tissue, 95%
482 CI [327.6, 943.5], $p = 0.001$). In CB-X rats, TNF- α administration led to higher levels of norepinephrine
483 in the spleen as compared to CB-X + vehicle (Mean difference = 212.4 pg mg^{-1} tissue, 95% CI [24.4,
484 400.4], $p = 0.025$), to SPL-X + vehicle (Mean difference = 452.0 pg mg^{-1} tissue, 95% CI [307.5, 596.6],
485 $p < 0.001$), and to SPL-X + TNF- α (Mean difference = 441.7 pg mg^{-1} tissue, 95% CI [298.1, 585.3], $p <$
486 0.001). SPL-X + vehicle animals also displayed lower levels of norepinephrine in the spleen compared
487 to SHAM + vehicle (Mean difference = $-312.6 \text{ pg mg}^{-1}$ tissue, 95% CI [-587.0, -38.1], $p = 0.030$) and
488 CB-X + vehicle (Mean difference = $-239.6 \text{ pg mg}^{-1}$ tissue, 95% CI [-413.5, -65.7], $p = 0.013$). Similarly,
489 the levels of norepinephrine in the spleen were also lower in SPL-X + TNF- α compared to SHAM +
490 vehicle (Mean difference = $-302.2 \text{ pg mg}^{-1}$ tissue, 95% CI [-574.7, -29.8], $p = 0.033$) and CB-X + vehicle
491 (Mean difference = $-229.3 \text{ pg mg}^{-1}$ tissue, 95% CI [-400.7, -57.9], $p = 0.014$).



492
493
494
495
496
497
498
499
500

Figure 6. Schematic model of the novel proposed neuroimmune mechanism. TNFR1, TNF- α receptors type I; CSN, carotid sinus nerve; IX cranial nerve, glossopharyngeal nerve; PG, petrosal ganglion; cNTS, commissural nucleus tractus solitarius; Glu, glutamate; RLVM, rostral ventrolateral medulla; IML, intermediolateral nucleus; Spl, splanchnic; NE, norepinephrine.

501 Discussion

502 In the present study, we provide a series of anatomical and functional evidence for the
503 existence of a previously unrecognized mechanism of neuroimmune interaction. The
504 main finding is that the carotid body is able to detect elevated levels of the pro-
505 inflammatory cytokine TNF- α in the blood and communicate with the central nervous
506 system via carotid sinus nerve afferents, activating RVLM-projecting cNTS excitatory
507 neurons that contribute to a counteracting sympathetic-mediated anti-inflammatory
508 response. These results advance our understanding of the complex mechanisms
509 underlying the bidirectional connection between the nervous and the immune systems.

510 Recently, the carotid bodies emerged as potential candidates for peripheral
511 detectors of inflammation. This possibility is supported by a growing number of studies
512 indicating that they are polymodal sensors, able to monitor the chemical composition
513 of the arterial blood. More specifically, these studies have shown that besides
514 promoting autonomic and respiratory adjustments in response to arterial hypoxemia
515 (i.e., peripheral chemoreflex), the carotid bodies can respond to several other
516 circulating stimuli such as leptin, angiotensin II, glucose, sodium chloride, insulin,
517 adrenaline, and, also, inflammatory mediators (Allen, 1998; da Silva et al., 2019;
518 Jendzjowsky et al., 2021, 2018; Katayama, 2016; Kumar and Prabhakar, 2012; Shin
519 et al., 2019; Thompson et al., 2016). Regarding inflammatory mediators, studies
520 reported that the carotid body of many species, including rats, cats and humans,
521 expresses receptors for lysophosphatidic acid (LPA), IL-1 β , IL-6, and TNF- α
522 (Fernández et al., 2008; Jendzjowsky et al., 2018; Mkrtchian et al., 2012; Wang et al.,
523 2002). Accordingly, in the present study, we employed a combination of
524 immunofluorescence and RNAscope fluorescent *in situ* hybridization that enabled the
525 detection and precise localization of TNFR1 mRNA molecules in the carotid body of
526 rats. Moreover, in addition to the anatomical evidence, previous functional studies
527 demonstrated that inflammation-related factors can impact carotid body activity
528 (Jendzjowsky et al., 2021, 2018; Shu et al., 2007), opening a wide range of possibilities
529 regarding the role of the carotid body in the context of neuroimmune interactions. For
530 instance, a recent study showed that LPA potently increased CSN activity in an
531 isolated perfused carotid body/carotid sinus nerve preparation (Jendzjowsky et al.,
532 2018). Furthermore, the same research group showed that the perfusion of the
533 isolated carotid body/carotid sinus nerve preparation with diverse pro-inflammatory

534 cytokines (IL-4, IL-5, IL-13, IL-1, IL-6, and TNF- α), one at a time or in combination,
535 also increased CSN activity (Jendzjowsky et al., 2021), confirming the unique ability
536 of the carotid body to sense and respond to inflammatory mediators. In our study, CSN
537 activity was recorded in vivo and TNF- α was given systemically (IV). We chose the IV
538 administration route because it better mimics a real scenario of systemic inflammation.
539 We observed a progressive and significant increase in CSN activity, indicating that the
540 carotid body could detect the elevated levels of TNF- α in the blood and alert the central
541 nervous system via afferent signals. The reasons by which TNF- α increased CSN
542 activity in a sustained manner (for at least 2 hours) are not clear, especially because
543 the half-life of TNF- α in the plasma is reported to be very short (few minutes) (Ma et
544 al., 2015; Simó et al., 2012). We hypothesize that the exogenous administered TNF-
545 α stimulated the synthesis and release of additional TNF- α , probably via direct
546 activation of splenic macrophages as suggested by our data (Figure 5) and/or by
547 indirect activation of liver Kupffer cells as observed during endotoxemia in rats
548 (Fonseca et al., 2021). This endogenously produced TNF- α could either sustain the
549 carotid body activation and, also, stimulate the synthesis of further TNF- α .

550 We found that besides increasing CSN activity, the intravenous administration
551 of TNF- α promoted the activation of cNTS neurons, the first relay site for carotid body
552 afferents. Notably, the systemic administration of TNF- α resulted in activation of the
553 cNTS neurons at the same rostro-caudal levels reported to be activated after carotid
554 body stimulation by hypoxia or intravenous KCN (Cruz et al., 2010; Kline et al., 2010;
555 Malheiros-Lima et al., 2020). These cNTS neurons, activated by carotid body
556 stimulation, project to several brain areas, including the RVLM, to control the
557 sympathetic nervous system (Kline et al., 2010; Koshiya and Guyenet, 1996). A
558 previous study observed that after 3 hours of hypoxia (10% O₂) exposure, a high
559 proportion of RVLM-projecting cNTS neurons were activated (Kline et al., 2010).
560 Furthermore, the authors injected anterograde tracers into the carotid body and
561 observed that carotid body afferents terminate in close apposition to the RVLM-
562 projecting cNTS neurons. Thus, this neural circuitry elegantly revealed by Kline et al.
563 (2010), along with previous data (Aicher et al., 1996; Koshiya and Guyenet, 1996),
564 provides a major neural pathway for hypoxia-induced sympathoexcitation. Of note, the
565 blockade of glutamatergic receptors in the NTS was shown to strongly reduce the
566 sympathetic responses to chemical stimulation of the carotid body (Ferreira et al.,
567 2018). Since in the present study, circulating TNF- α induced the activation of RLVM-

568 projecting cNTS glutamatergic neurons at the same rostro-caudal levels reported in
569 the literature (Cruz et al., 2010; Kline et al., 2010; Malheiros-Lima et al., 2020) and,
570 because carotid body ablation almost abolished the activation of these neurons, we
571 believe that TNF- α might be stimulating a similar neural pathway (carotid body-cNTS-
572 RVLM) activated by hypoxia to increase sympathetic activity. It is important to highlight
573 that more than a half of c-FOS positive neurons observed in SHAM rats treated with
574 TNF- α were not co-localized with FG (non-RVLM-projecting). We hypothesize that
575 these neurons project to other nuclei involved in sympathetic modulation, such as the
576 PVN, regions involved in respiratory control, and vagal nuclei (Luise King et al., 2012;
577 Malheiros-Lima et al., 2020; Neff et al., 1998; Willis et al., 1996; Zera et al., 2019). In
578 fact, recent studies suggested that inflammation-induced carotid body stimulation
579 could also activate brainstem vagal nuclei (nucleus ambiguus and dorsal motor
580 nucleus of the vagus) to increase parasympathetic activity (Jendzjowsky et al., 2021,
581 2018). Therefore, the results of the present and previous studies suggest that the
582 carotid body detects circulating inflammatory mediators and activates central
583 autonomic areas to modulate sympathetic and/or parasympathetic functions.

584 Our study shows that the TNF- α -induced activation of a sympathoexcitatory
585 circuit (carotid body-cNTS-RVLM) resulted in increased SNA as revealed by
586 simultaneous recordings of splanchnic, renal and lumbar SNA. To the best of our
587 knowledge, this is the first study describing the effects of circulating TNF- α , an
588 important inflammatory mediator, on the activity of three different sympathetic nerves
589 recorded simultaneously in vivo. Previous studies have already demonstrated that
590 circulating TNF- α increases renal SNA in rats (Wei et al., 2013; Zhang et al., 2003).
591 However, since sympathetic outflows to other tissues/organs have distinct functions
592 and can be differentially regulated (Morrison, 2001; Tromp et al., 2018), it becomes
593 relevant to study the effects of TNF- α on sympathetic outflows directed to other targets
594 besides the kidneys. Here, we found that TNF- α promoted a generalized activation of
595 the sympathetic nervous system, increasing splanchnic, renal, and lumbar SNA in
596 carotid body-intact rats. The removal of the afferent inputs from the carotid bodies (by
597 bilateral carotid body ablation) blunted, in part, this TNF- α -induced sympathetic
598 activation, consistent with the attenuated activation of RLVM-projecting cNTS neurons
599 observed in CB-X rats (Figure 3C – E). Interestingly, the blunting effect of carotid body
600 ablation was significant only on splanchnic SNA. Therefore, our data indicate that
601 increased circulating TNF- α activates a carotid body-cNTS-RVLM neural circuit that

602 selectively controls splanchnic SNA in this condition. It is noteworthy that a previous
603 study reported that the increase in renal SNA following the systemic administration of
604 TNF- α was largely attenuated in rats with lesions of the subfornical organ (Wei et al.,
605 2013). It suggests that splanchnic, renal, and lumbar SNA might be under the control
606 of different neural routes and might have different functions in the course of TNF- α -
607 driven inflammation.

608 In this context, some studies have suggested that the splanchnic sympathetic
609 nerves play an important immunomodulatory role during endotoxemia-induced
610 systemic inflammation (Lankadeva et al., 2020; Martelli et al., 2014). For instance, it
611 was demonstrated that acute endotoxemia induced by intravenous administration of
612 lipopolysaccharide (LPS) significantly increased plasma levels of TNF- α after 90
613 minutes in rats (Martelli et al., 2014). In parallel, this LPS administration potently
614 increased splanchnic SNA. Notably, when LPS was given to rats subjected to the
615 bilateral section of the splanchnic sympathetic nerves, the plasma TNF- α levels
616 increased 5 times more than those of intact rats (Martelli et al., 2014). Together, these
617 results indicate that during LPS-induced systemic inflammation, the splanchnic SNA
618 increases to counteract the ongoing inflammation in a kind of negative feedback reflex.
619 Since, in the present study, the elevated circulating TNF- α activated a carotid body-
620 cNTS-RVLM neural circuit to increase splanchnic SNA, we hypothesized that this
621 mechanism could be a neuroimmune reflex to counteract the TNF- α -induced
622 inflammation. To test this hypothesis, we removed either the detection/afferent arm
623 (i.e., the carotid bodies) or the efferent arm (i.e., the splanchnic sympathetic nerves)
624 of this potential neuroimmune reflex and subjected these animals (and SHAM control
625 animals) to systemic injections of TNF- α or vehicle. After 2 hours, we quantified the
626 levels of TNF- α , IL-6, and IL-10 in the blood and in the spleen as well as the levels of
627 norepinephrine in the spleen. We found that in SHAM rats, the administration of TNF-
628 α significantly increased the plasma levels of TNF- α and slightly increased the spleen
629 levels of TNF- α compared to vehicle-injected SHAM rats. In addition, TNF- α
630 administration tended to increase spleen norepinephrine levels in SHAM animals as
631 compared to its vehicle-treated counterparts (Figure 5H, $p = 0.06$), consistent with our
632 data showing a TNF- α induced splanchnic SNA activation. Interestingly, in rats
633 subjected to either carotid body ablation or splanchnic sympathetic denervation, the
634 administration of TNF- α resulted in exacerbated levels of pro-inflammatory cytokines
635 in the plasma and the spleen, supporting the idea that both the detection/afferent arm

636 and the efferent arm are important components of a neuroimmune regulatory
637 mechanism that detects and modulates acute inflammation through sympathetic
638 activation towards the spleen. Disrupting the afferent/detection component (carotid
639 body ablation) resulted in a peculiar elevation of all quantified cytokines, including IL-
640 10 (an anti-inflammatory cytokine). The reason for this elevation in plasma IL-10 in
641 CB-X rats treated with TNF- α is not clear. This could result from the fact that carotid
642 body ablation eliminated only part of the autonomic circuits toward the spleen, possible
643 preserving and/or amplifying other counter-inflammatory mechanisms. In fact, the
644 administration of TNF- α in CB-X rats, still activated splanchnic SNA and resulted in a
645 significant increase in splenic levels of norepinephrine compared to vehicle-injected
646 CB-X rats. However, the TNF- α -induced splanchnic SNA activation and
647 norepinephrine release in the spleen were attenuated in CB-X rats compared to SHAM
648 rats, which could explain, at least in part, the exacerbated inflammatory status
649 observed in the animals lacking the carotid bodies. Differently, the interruption of the
650 efferent component (splanchnic sympathetic denervation) completely blocked the
651 sympathetic signalling to the spleen, removing the norepinephrine “inhibitory tonus”
652 on cytokine production by splenic macrophages, resulting in elevated splenic cytokine
653 levels even in those animals administered with saline. Collectively, our data suggest
654 the existence of an intrinsic and physiological anti-inflammatory reflex that depends
655 on a detection/afferent arm (i.e., the carotid bodies and the carotid sinus nerve), on a
656 central integrative pathway (i.e., RVLM-projecting cNTS neurons), and on an
657 effector/efferent arm (i.e., splanchnic sympathetic nerves) that modulates the splenic
658 production of cytokines through norepinephrine release.

659 The findings of the present study are novel and place the carotid body as a
660 critical player in the context of neuroimmune interactions. In the last years, the
661 contribution of the carotid bodies to sympathetic overactivity has been implicated in
662 the pathophysiology of several diseases such as sleep apnoea, hypertension, and
663 heart failure (Marcus et al., 2014; McBryde et al., 2013; Melo et al., 2019; Narkiewicz
664 et al., 2016; Niewinski et al., 2017; Yuan et al., 2016). In these conditions, exaggerated
665 tonic CSN activity leads to chronic activation of the sympathetic nervous system, often
666 associated with a poor prognosis. Here, we found that the acute carotid body-mediated
667 sympathetic activation induced by intravenous TNF- α is likely to be beneficial because
668 it exerted a counteracting anti-inflammatory reflex. However, it is possible that in
669 chronic pathological inflammatory conditions, the long-term activation of this carotid

670 body-dependent neuroimmune circuit leads to side effects because it generates an
671 aberrant tonic CSN input to central sympathetic networks, leading to sustained
672 sympathetic overactivity to multiple target organs. This possibility raises an intriguing
673 question on whether circulating inflammatory factors could trigger the carotid body-
674 mediated sympathetic overactivity observed in diseases such as hypertension
675 (McBryde et al., 2013; Narkiewicz et al., 2016) and heart failure (Marcus et al., 2014;
676 Niewinski et al., 2017) since these conditions are associated with increased systemic
677 inflammation (Bautista et al., 2005; Norlander et al., 2018; Rauchhaus et al., 2000;
678 Sesso et al., 2015). On the other hand, defects in the carotid body-mediated
679 neuroimmune reflex described here, could impair the ability to regulate the levels of
680 inflammatory mediators in the bloodstream, amplifying systemic inflammation.
681 Nevertheless, further investigations are needed to clarify the beneficial or detrimental
682 effects following the activation/inactivation of the neuroimmune mechanism described
683 in the present study under different conditions and to explore its therapeutic potential
684 in the treatment of inflammatory diseases.

685

686

687 **Methods**

688 **Animals and ethical approval**

689 All experimental procedures were reviewed and approved by the Ethical Committee in
690 Animal Experimentation of the Araraquara School of Dentistry, São Paulo State
691 University (protocol nº 17/2019) and conducted following the Guide for the Care and
692 Use of Laboratory Animals from the Brazilian National Council for Animal
693 Experimentation Control. Experiments were performed on adult male *Holtzman* rats
694 (320 - 400 g) obtained from the Animal Care Unit of the São Paulo State University
695 (Araraquara, SP, Brazil). The animals were housed in collective cages (2 - 4
696 animals/cage), provided with chow and water *ad libitum*, and maintained under
697 controlled conditions of temperature ($22 \pm 1^\circ\text{C}$), humidity (50 - 60%) in a 12:12 hours
698 light/dark cycle.

699

700

701

702

703 **General procedures**

704 All surgical procedures were performed under aseptic conditions. The appropriate
705 depth of anesthesia was confirmed by the absence of withdrawal reflex and corneal
706 reflexes in response to pinching the toe. Throughout the surgical procedures and the
707 experimental protocols performed under anesthesia (described below), the body
708 temperature was measured by a rectal probe and maintained at $37 \pm 0.5^{\circ}\text{C}$ with a
709 water-circulating heating pad.

710

711

712 **Experiment 1: Expression of TNF- α receptor type I in carotid body glomus cells**

713 Rats were deeply anesthetized with isoflurane (5% in 100 O₂) and subjected to
714 transcatheter perfusion with cold phosphate-buffered saline (PBS, 10 mM, pH 7.4, 100
715 mL/100 g BW) followed by paraformaldehyde (PFA, 4% in PBS, 100 mL/100 g BW).
716 Whole carotid bifurcations containing the carotid bodies were collected as previously
717 described (Pijacka et al., 2018) and fixed in PFA for 24 hours at 4^o C. Next, carotid
718 bifurcations were transferred to 10% sucrose solution and kept at 4^o C until the tissue
719 sinks. This procedure was repeated with 20% and 30% sucrose solutions. Carotid
720 bifurcations were frozen in Tissue Freezing Medium (Triangle Biomedical Sciences,
721 Durham, NC, USA) using dry ice, sectioned at 10 μm in a cryostat and mounted on
722 microscope slides (Superfrost Plus, Fisher Scientific, Pittsburgh, PA, USA). To
723 evaluate the expression of TNF- α receptor type I in the carotid bodies, a fluorescent
724 *in situ hybridization* assay (RNAscope, Advanced Cell Diagnostics, Newark, CA, USA)
725 was used. The assay was performed according to the manufacturer instructions
726 (document #323100-USM, available at [https://acdbio.com/documents/product-](https://acdbio.com/documents/product-documents)
727 [documents](https://acdbio.com/documents/product-documents)) and the following materials were used: RNAscope Multiplex Fluorescent
728 Detection Reagents v2 (product #323110), the kit RNAscope H₂O₂ and Protease
729 Reagents (product #322381), the RNAscope probe for TNF- α receptor type I (product
730 #408111) and the TSA Cyanine 3 Plus Evaluation kit (product #NEL744001KT, Akoya
731 Biosciences, Boston, MA, USA). After completing the fluorescent *in situ hybridization*
732 protocol, an immunofluorescence protocol for tyrosine hydroxylase (TH) was
733 performed to identify carotid body glomus cells. First, the slides were incubated in a
734 blocking solution (0.1 M PBS, 10% normal horse serum, and 0.3% Triton X-100) for
735 20 min and subsequently rinsed 3 x 10 minutes in 0.1 M PBS at room temperature.
736 Then, the slides were incubated in primary antibody (Mouse anti-TH antibody, 1:1000,

737 product #MAB5280, Millipore, Billerica, MA, USA) for 1 hour at room temperature and
738 36 hours at 4° C. After rinsing in PBS, the slides were incubated in secondary antibody
739 (Alexa Fluor 488 donkey anti-mouse antibody, 1:200, product #R37114, Molecular
740 Probes-Life Technologies, Eugene, OR, USA) for 4 hours at room temperature. The
741 slides were rinsed in PBS, the excess liquid was drained, mounting medium
742 (Fluoromount) was dropped on the tissue and slides were covered with glass
743 coverslips (Fisherfinest). Images were acquired using a laser scanning confocal
744 microscope (LSM800, Zeiss). For presentation purposes (color-blind safe) images
745 were pseudo-colored and representative figures were prepared using the Zen 2
746 software (Blue edition, Zeiss).

747

748

749 **Experiment 2: Effects of circulating TNF- α on carotid sinus nerve afferent** 750 **activity**

751 Animals were anesthetized with isoflurane (Induction 5% and maintenance 2.5% in
752 100% O₂) and subjected to femoral artery and vein catheterizations for arterial blood
753 pressure (ABP) monitoring and drug administration, respectively, using polyethylene
754 catheters (PE-50 attached to PE-10, Becton Dickinson, Sparks, MD, USA). Next,
755 through a midline neck incision, the trachea was cannulated, and animals were
756 artificially ventilated with a rodent ventilator (model 7025, Ugo Basile, Gemonio, VA,
757 Italy). End-tidal CO₂ was maintained between 4 - 5% (Capstar-100 carbon dioxide
758 analyzer, CWE, Ardmore, PA, USA) by adjusting tidal volume (0.7 - 0.8 mL/100 g of
759 body weight) and respiratory rate (60 - 80 bpm). Isoflurane was slowly replaced with
760 urethane anesthesia (1.2 - 1.4 g/kg of body weight, IV) given over 20 - 25 minutes.
761 Then, O₂ concentration in ventilated air was switched to 50% O₂ (balance N₂) and this
762 condition was kept until the end of the experiments. This slightly hyperoxic
763 concentration was chosen because it ensures a stable preparation without silencing
764 carotid body activity as 100% O₂ would do (Kim et al., 2018; Schultz et al., 2007) and
765 to avoid any period of hypoxia during the experimental protocol.

766 Then, animals were prepared for recordings of CSN afferent activity. The left
767 carotid sinus nerve was identified, carefully isolated, and cut centrally at its junction to
768 the glossopharyngeal nerve. CSN activity was recorded using bipolar suction
769 electrodes and signals were filtered (100 - 3000 Hz), amplified (10,000 X) and digitally

770 sampled (10 kHz). After baseline recordings, TNF- α (500 ng in 0.5 mL sterile saline,
771 IV; PeproTech, Rocky Hill, NJ, USA) was administered and CSN activity was recorded
772 for additional 2 hours. This dose was chosen based on previous works studying the
773 effects of TNF- α on renal SNA in vivo (Zhang et al. 2003, Wei et al. 2015). Reliability
774 of CSN activity was confirmed at the end of experiments by a robust increase in
775 electrical activity during the exposure to hypoxia (10% O₂) for 60 - 90 seconds.

776
777

778 **Experiment 3: Neuroanatomical identification of carotid body-related central** 779 **sympathoexcitatory pathways activated by circulating TNF- α**

780 First, the animals were anesthetized with a mixture of ketamine (80 mg kg⁻¹, IP; União
781 Química Farmacêutica Nacional S/A, Embu-Guaçu, SP, Brazil) and xylazine (8 mg kg⁻¹,
782 IP; Hertape Calier Saúde animal S/A, Juatuba, MG, Brazil), and placed in a
783 stereotaxic frame (David Kopf instruments, Tujunga, CA, USA). The retrograde tracer
784 FluoroGold (FG, 2%, Fluorochrome, Denver, CO, USA) diluted in artificial
785 cerebrospinal fluid (aCSF) was then bilaterally injected (40 nL) into the RVLM.
786 Microinjections were performed with a pressure microinjector (Picospritzer III, Parker
787 Hannifin, Hollis, NH, USA) using glass micropipettes. After each injection, the
788 micropipette was kept in place for 2 minutes to prevent FG reflux. The coordinates
789 used to target the RVLM were: 3.5 mm caudal from Lambda, 1.8 - 2.0 mm lateral from
790 the midline, and 9.4 mm ventral from the skull surface. After injections, the skin
791 incisions were sutured and the animals received anti-inflammatory ketoprofen (3 mg
792 kg⁻¹, SC) and antibiotics penicillin (50,000 IU, IM). This treatment was repeated every
793 24 hours for 3 days.

794 After 6 days recovery, animals were subjected to bilateral carotid body ablation
795 (CB-X group) or Sham procedure (Sham group) and femoral artery/vein
796 catheterizations. Carotid body ablation was performed by combining two previously
797 described methods (Katayama et al., 2015; Pijacka et al., 2018). Briefly, animals were
798 anesthetized with ketamine/xylazine as previously described. The carotid body
799 arteries were ligated and cut, followed by surgical removal of the carotid bodies on
800 both sides. In this procedure, the carotid sinus nerve is maintained intact, preserving
801 carotid baroreflex function (Pijacka et al., 2018). Sham procedure consisted in isolation
802 of carotid body arteries and carotid bodies, but these structures were kept intact. Neck
803 incisions were closed with sutures. Femoral artery/vein catheters were tunneled

804 subcutaneously, exteriorized and fixed in the interscapular region as previously
805 described (Katayama et al., 2019). After surgeries, animals were treated with
806 antibiotics and anti-inflammatory for 3 days as described before. To maintain catheters
807 patency, arterial and venous catheters were flushed every day with heparinized saline
808 (arterial: 500 U/mL, venous: 40 U/mL). Three days after surgery, ABP was recorded
809 in unanesthetized rats under baseline conditions and in response to potassium
810 cyanide (KCN; 40 ug/animal, IV) to verify the efficacy of carotid body ablation in CB-X
811 group and the integrity of carotid bodies in SHAM group. Successful bilateral carotid
812 body ablation was confirmed by the lack of cardiovascular responses to KCN (figure
813 supplement 1A – B). Rats were allowed to recover for 3 days before the next
814 experimental protocol.

815 On the day of the experiment (12 days after FG microinjections), rats were
816 administered with TNF- α (500 ng in 0.5 mL sterile saline, IV) and left undisturbed for
817 2 hours. Next, rats were deeply anesthetized with urethane (IV) and transcardially
818 perfused with PBS followed by PFA. Brains were collected and fixed in PFA for 12
819 hours at 4^o C. Brains were then transferred to 20% sucrose solution and maintained
820 at 4^o C until the tissue sinks. Finally, brains were frozen in Tissue Freezing Medium
821 (Triangle Biomedical Sciences, Durham, NC, USA) and coronal brain slices (30 μ m)
822 containing the cNTS and the RVLM were obtained on a cryostat. The RVLM sections
823 were mounted on microscope slides (Superfrost Plus, Fisher Scientific, Pittsburgh, PA,
824 USA) and used to confirm the location of FluoroGold microinjections within RVLM
825 region (From 12.48 mm to 12.00 mm caudal to bregma, ventral to the compact
826 formation of the Nucleus Ambiguus) accordingly to the rat brain in stereotaxic
827 coordinates atlas (Paxinos and Charles Watson, 2007). The cNTS sections were
828 stored in cryoprotectant solution at -20^o C until processing for c-FOS and VGlut2
829 immunofluorescence as described below.

830 Briefly, sections were first rinsed in 0.1 M PBS for 10 minutes followed by
831 incubation in blocking solution (0.1 M PBS, 10% normal horse serum, and 0.3% Triton
832 X-100) for 20 min at room temperature. After rinsing 3 x 10 minutes in 0.1 M PBS at
833 room temperature, slides were incubated in primary antibodies for c-FOS (1:1000,
834 rabbit anti-c-FOS polyclonal antibody, product #sc-52, Santa Cruz Biotechnology,
835 Santa Cruz, CA, USA) and for VGlut2 (1:2000, guinea pig anti-VGlut2 polyclonal
836 antibody, product #AB2251-I, Millipore, Temecula, CA, USA) for 1 hour at room

837 temperature plus 36 hours at 4^o C. After rinsing in PBS, slides were incubated in
838 secondary antibodies against rabbit (1:400, donkey anti-rabbit Alexa Fluor 594,
839 product #A-21207, Molecular Probes-Life Technologies, Eugene, OR, USA) and
840 against anti-guinea pig (1:400, donkey anti-guinea pig Alexa Fluor 488, product #706-
841 545-148, Jackson ImmunoResearch Inc, West Grove, PA, USA) for 4 hours at room
842 temperature. Slides were rinsed in PBS, the excess liquid was drained, mounting
843 medium (Fluoromount, product # F4680, Sigma, St. Louis, MO, USA) was dropped on
844 the tissue and slides were covered with glass coverslips (Fisherfinest, product
845 #125485M, Fisher Scientific).

846 Images were acquired using a laser scanning confocal microscope (LSM800
847 with airyscan, Zeiss, Jena, TH, Germany). Quantification of retrograde labeled FG
848 cells, c-FOS positive cells, FG/c-FOS cells, and FG/c-FOS/VGluT2 cells within the
849 cNTS were performed on brainstem sections from three different rostro-caudal levels
850 (between 14.76 mm to 14.04 mm caudal to bregma). These levels were chosen based
851 on studies demonstrating NTS regions that are activated after carotid body stimulation
852 (Cruz et al., 2010; Kline et al., 2010; Malheiros-Lima et al., 2020). As anatomical
853 landmarks to identify the cNTS levels, we used: the area postrema, the central canal,
854 the gracile nucleus, and the hypoglossal nucleus. Cell counting was performed on
855 ImageJ software (U.S. National Institutes of Health, Bethesda, MD, USA) and
856 representative figures were prepared using the Zen 2 software (Blue edition, Zeiss).

857

858

859 **Experiment 4: Sympathetic responses to circulating TNF- α in Sham and carotid** 860 **body-ablated (CB-X) rats**

861 Animals were anesthetized, subjected to femoral artery/vein catheterizations,
862 tracheotomized and continuously ventilated with 50% O₂ (balance N₂) as described in
863 *Experiment 2*. Next, animals were subjected to bilateral carotid body ablation or sham
864 surgery as described in *Experiment 3*. All animals were then prepared for
865 simultaneous recordings of lumbar, renal, and splanchnic sympathetic nerve activity
866 (SNA). Lumbar sympathetic nerve was isolated through a midline laparotomy and
867 retraction of vena cava, while renal and splanchnic sympathetic nerves were isolated
868 through a retroperitoneal incision and careful retraction of the left kidney. Each
869 sympathetic nerve was placed on a bipolar stainless-steel electrode and insulated with

870 KWIK-SIL (World Precision Instruments, Sarasota, FL, USA). The raw SNA signals
871 were filtered (100 - 1000 Hz), amplified (10,000 X) using biological amplifiers (P511
872 AC Amplifier, Grass Technologies, Warwick, RI, USA), displayed on oscilloscopes
873 (TDS 2022, Tektronix, Beaverton, OR, USA) and digitally sampled (2 kHz) by a data
874 acquisition system (Micro 1401, Cambridge Electronic Design Limited). All incisions
875 were closed with surgical clips (Fine Science Tools, Foster City, CA, USA).

876 After stabilization (~30 minutes after the end of surgical procedures), baseline
877 recordings of ABP, lumbar, renal and splanchnic SNA were performed. Next, TNF- α
878 (500 ng in 0.5 mL sterile saline, IV) was administered and ABP and SNA were
879 recorded for additional 2 hours. At the end of the experiments, carotid body ablation
880 was confirmed by the absence of blood pressure and SNA responses to KCN (40
881 ug/animal, IV) and these results are presented in figure supplement 2A – B.

882

883 **Experiment 5: Plasma and spleen levels of pro-inflammatory cytokines following** 884 **intravenous TNF- α in SHAM, CB-X and SPL-X rats**

885 Rats were anesthetized with ketamine/xylazine and prepared accordingly one of the
886 following experimental groups: 1) CB-X: Animals were subjected to bilateral ablation
887 of the carotid bodies; 2) SPL-X: Animals were subjected to splanchnic denervation
888 through celiac ganglionectomy as previously reported in the literature (Asirvatham-
889 Jeyaraj et al., 2021; Li et al., 2010). Briefly, after a midline laparotomy, the visceral
890 organs were gently retracted, and the celiac ganglion was localized and surgically
891 removed using blunt forceps. 3) SHAM: The carotid bodies and the celiac ganglion
892 were localized and manipulated, but these structures were kept intact. All animals
893 were allowed to recover for 6 days. Next, animals were subjected to femoral
894 artery/vein catheterizations. The efficacy of carotid body ablation in CB-X group and
895 the integrity of carotid bodies in SHAM and SPL-X groups was verified three days after
896 catheterizations and these results are presented in figure supplement 3A – B. Then,
897 rats were allowed to recover for additional 3 days before the experimental protocol.

898 The experimental protocol consisted in the administration of TNF- α (500 ng, IV)
899 or vehicle (sterile saline, IV) in SHAM, CB-X and SPL-X rats. After 2 hours, rats were
900 deeply anesthetized for tissue collection. Blood was collected into EDTA-containing
901 tubes, centrifuged (1500 rpm for 10 min) at 4^o C and the plasma was aliquoted and
902 stored at -80^o C. Spleen was harvested, flash frozen using liquid nitrogen and stored
903 at -80^o C.

904 The spleen samples were homogenized in PBS using a Polytron tissue
905 homogenizer, and then centrifuged at 10,000 rpm for 2 min at 4 °C. The plasma and
906 splenic levels of cytokines were quantified by enzyme-linked immunosorbent assay
907 (ELISA) using commercial kits DuoSet ELISA Development Systems (R&D Systems,
908 Minneapolis, MN, USA) for TNF- α (catalog #DY510), IL-6 (catalog #DY506), and IL-
909 10 (catalog #DY522) and following the user manual instructions. The results were
910 expressed as cytokine concentration in pg/mL and pg/mg of protein, based on
911 standard curves, respectively. Spleen norepinephrine was measured as previously
912 described (Garofalo et al., 1996) using HPLC (LC20AT-Shimadzu Proeminence)
913 coupled to an electrochemical detector (Decade Lite-Antec Scientific) with a 5- μ m
914 Spherisorb ODS-2 reversed-phase column (Sigma-Aldrich) and the results were
915 expressed as norepinephrine concentration in ng/g of tissue.

916

917

918 **Statistical analysis**

919 All statistical analyses were performed using IBM SPSS Statistics (version 25, IBM
920 corporation). Data are reported as means \pm SEM. The significance level was set at p
921 < 0.05 , unless otherwise stated. No outliers were found as assessed by boxplot
922 analyses. *Experiment 2:* To examine differences between means within the same
923 group over time, the one-way repeated measures analysis of variance (ANOVA)
924 followed by post hoc analysis with Bonferroni adjustment was performed. The normal
925 distribution of the data was verified and confirmed by the Shapiro-Wilk test, and the
926 Mauchly's test indicated that the assumption of sphericity has not been violated.
927 *Experiment 3:* To determine differences between two groups at a single time-point, we
928 first assessed the distribution of the data using the Shapiro-Wilk test and the
929 homogeneity of variances using the Levene's test. For normally distributed data with
930 homogenous variances, an unpaired two-tailed Student's t -test was performed. In
931 cases in which the data was normally distributed but the assumption of homogeneity
932 of variances was violated, an unpaired two-tailed Welch's t -test was used. When data
933 was not normally distributed, an unpaired two-tailed Mann-Whitney U -test was applied.
934 *Experiment 4:* To determine group x time interactions, a two-way repeated measures
935 ANOVA was conducted. In this case, the normal distribution of the studentized
936 residuals was verified and confirmed by the Shapiro-Wilk test. The sphericity for the
937 interaction term was assessed by the Mauchly's test. When the assumption of

938 sphericity was violated, the Greenhouse-Geisser correction was used and the
939 estimated epsilon (ϵ) value was reported. Once statistically significant group x time
940 interactions were detected, simple main effects of group were analyzed using repeated
941 measures general linear models with Bonferroni adjustment. *Experiment 5*: To
942 examine group x treatment interactions and main effects of group, a two-way ANOVA
943 with Bonferroni post hoc was performed. The distribution of the residuals was
944 examined by the Shapiro-Wilk test. The homoscedasticity was analyzed by the
945 Levene's test and by plotting the residuals against the predicted values in a simple
946 scatterplot. If the assumptions of normal distribution and/or homoscedasticity were
947 violated, the dependent variable was log-transformed when appropriate. When both
948 the assumptions of normality and homoscedasticity (requirements for two-way
949 ANOVA) were not satisfied even after transformation, a Kruskal-Wallis followed by
950 Mann-Whitney *U*-tests for pairwise comparisons between groups were performed. In
951 these cases, a Bonferroni adjustment to alpha values was applied and the statistical
952 significance was accepted at the $p < 0.003$ level. In cases in which only the assumption
953 of homoscedasticity was violated, a Welch's ANOVA followed by a Games-Howell
954 post hoc was used to compare groups.

955

956

957

958

959

960

961

962

963

964

965

966

967

968

969

970

971

972 **Acknowledgments**

973 The authors thank Lilian do Carmo Heck for the excellent technical assistance. This
974 work was funded by the São Paulo Research Foundation (FAPESP; grants
975 #2019/11196-0 and #2015/23467-7), CNPq, and PROPE-UNESP.

976

977 **Author contributions**

978 P.L.K. and E.C. conceived and designed research. P.L.K. performed all in vivo
979 experiments. P.L.K. and I.P.L. performed immunofluorescence and in situ
980 hybridization. A.K. and J.P.M.L. performed ELISA. L.C.C.N. performed HPLC
981 measurements. P.L.K., I.P.L., A.K., and J.P.M.L. analyzed data. P.L.K., I.P.L., A.K.,
982 D.B.Z, and E.C. interpreted data. P.L.K. and A.K. drafted the manuscript. P.L.K., I.P.L.,
983 A.K., J.P.M.L., F.Q.C., L.C.C.N., J.V.M., D.B.Z., D.S.A.C., and E.C. edited and revised
984 the manuscript. P.L.K., I.P.L., A.K., J.P.M.L., F.Q.C., L.C.C.N, J.V.M., D.B.Z.,
985 D.S.A.C., and E.C. read and approved the final version of the manuscript.

986

987 **Competing interests**

988 The authors declare no competing interests.

989

990 **Materials & correspondence**

991 Correspondence and requests for materials should be addressed to P.L.K. and/or E.C.

992

993

994

995

996

997

998

999

1000

1001

1002

1003

1004 **REFERENCES**

1005

1006 Abe C, Inoue T, Inglis MA, Viar KE, Huang L, Ye H, Rosin DiL, Stornetta
1007 RL, Okusa MD, Guyenet PG. 2017. C1 neurons mediate a stress-
1008 induced anti-inflammatory reflex in mice. *Nature Neuroscience*
1009 **20**:700–707. doi:10.1038/nn.4526

1010 Aicher SA, Saravay RH, Cravo S, Jeske I, Morrison SF, Reis DJ, Milner
1011 TA. 1996. Monosynaptic projections from the nucleus tractus solitarii
1012 to C1 adrenergic neurons in the rostral ventrolateral medulla:
1013 Comparison with input from the caudal ventrolateral medulla. *Journal*
1014 *of Comparative Neurology* **373**:62–75. doi:10.1002/(SICI)1096-
1015 9861(19960909)373:1<62::AID-CNE6>3.0.CO;2-B

1016 Allen AM. 1998. Angiotensin AT1 receptor-mediated excitation of rat
1017 carotid body chemoreceptor afferent activity. *Journal of Physiology*
1018 **510**:773–781. doi:10.1111/j.1469-7793.1998.773bj.x

1019 Asirvatham-Jeyaraj N, Gauthier MM, Banek CT, Ramesh A, Garver H,
1020 Fink GD, Osborn JW. 2021. Renal Denervation and Celiac
1021 Ganglionectomy Decrease Mean Arterial Pressure Similarly in
1022 Genetically Hypertensive Schlager (BPH/2J) Mice. *Hypertension*
1023 **519**–528. doi:10.1161/HYPERTENSIONAHA.119.14069

1024 Bassi GS, Dias DPM, Franchin M, Talbot J, Reis DG, Menezes GB,
1025 Castania JA, Garcia-Cairasco N, Resstel LBM, Salgado HC, Cunha
1026 FQ, Cunha TM, Ulloa L, Kanashiro A. 2017. Modulation of
1027 experimental arthritis by vagal sensory and central brain stimulation.
1028 *Brain, Behavior, and Immunity* **64**:330–343.
1029 doi:10.1016/j.bbi.2017.04.003

1030 Bassi GS, Kanashiro A, Coimbra NC, Terrando N, Maixner W, Ulloa L.
1031 2020. Anatomical and clinical implications of vagal modulation of the
1032 spleen. *Neuroscience and Biobehavioral Reviews* **112**:363–373.

- 1033 doi:10.1016/j.neubiorev.2020.02.011
- 1034 Bautista LE, Vera LM, Arenas IA, Gamarra G. 2005. Independent
1035 association between inflammatory markers (C-reactive protein ,
1036 interleukin-6 , and TNF- a) and essential hypertension 149–154.
1037 doi:10.1038/sj.jhh.1001785
- 1038 Borovikova L V., Ivanova S, Zhang M, Yang H, Botchkina GI, Watkins
1039 LR, Wang H, Abumrad N, Eaton JW, Tracey KJ. 2000. Vagus nerve
1040 stimulation attenuates the systemic inflammatory response to
1041 endotoxin. *Nature* **405**:458–462. doi:10.1038/35013070
- 1042 Chang EH, Chavan SS, Pavlov VA. 2019. Cholinergic control of
1043 inflammation, metabolic dysfunction, and cognitive impairment in
1044 obesity-associated disorders: Mechanisms and novel therapeutic
1045 opportunities. *Frontiers in Neuroscience* **13**:1–13.
1046 doi:10.3389/fnins.2019.00263
- 1047 Colombari E, Menani J V, Talman WT. 1996. Commissural NTS
1048 contributes to pressor responses to glutamate injected into the
1049 medial NTS of awake rats. *American Journal of Physiology-*
1050 *Regulatory, Integrative and Comparative Physiology* **270**:R1220–
1051 R1225. doi:10.1152/ajpregu.1996.270.6.R1220
- 1052 Cruz J de C, Bonagamba LGH, Stern JE, Machado BH. 2010. Fos
1053 expression in the NTS in response to peripheral chemoreflex
1054 activation in awake rats. *Autonomic Neuroscience: Basic and Clinical*
1055 **152**:27–34. doi:10.1016/j.autneu.2009.08.016
- 1056 da Silva EF, Bassi M, Menani JV, Colombari DSA, Zoccal DB, Pedrino
1057 GR, Colombari E. 2019. Carotid bodies contribute to
1058 sympathoexcitation induced by acute salt overload. *Experimental*
1059 *Physiology* **104**:15–27. doi:<https://doi.org/10.1113/EP087110>
- 1060 Erickson JT, Millhorn DE. 1994. Hypoxia and electrical stimulation of the
1061 carotid sinus nerve induce fos-like immunoreactivity within

- 1062 catecholaminergic and serotonergic neurons of the rat brainstem.
1063 *Journal of Comparative Neurology* **348**:161–182.
1064 doi:10.1002/cne.903480202
- 1065 Fernández R, González S, Rey S, Cortés PP, Maisey KR, Reyes EP,
1066 Larraín C, Zapata P. 2008. Lipopolysaccharide-induced carotid body
1067 inflammation in cats: Functional manifestations, histopathology and
1068 involvement of tumour necrosis factor- α . *Experimental Physiology*
1069 **93**:892–907. doi:10.1113/expphysiol.2008.041152
- 1070 Ferreira CB, Cravo SL, Stocker SD. 2018. Airway obstruction produces
1071 widespread sympathoexcitation: role of hypoxia, carotid
1072 chemoreceptors, and NTS neurotransmission. *Physiological Reports*
1073 **6**. doi:10.14814/phy2.13536
- 1074 Filiano AJ, Xu Y, Tustison NJ, Marsh RL, Baker W, Smirnov I, Overall
1075 CC, Gadani SP, Turner SD, Weng Z, Peerzade SN, Chen H, Lee
1076 KS, Scott MM, Beenhakker MP, Litvak V, Kipnis J. 2016.
1077 Unexpected role of interferon- γ 3 in regulating neuronal connectivity
1078 and social behaviour. *Nature* **535**:425–429.
1079 doi:10.1038/nature18626
- 1080 Fonseca MT, Moretti EH, Marques LMM, MacHado BF, Brito CF,
1081 Guedes JT, Komegae EN, Vieira TS, Festuccia WT, Lopes NP,
1082 Steiner AA. 2021. A leukotriene-dependent spleen-liver axis drives
1083 TNF production in systemic inflammation. *Science Signaling* **14**.
1084 doi:10.1126/scisignal.abb0969
- 1085 Garofalo MAR, Kettelhut IC, Roselino JES, Migliorini RH. 1996. Effect of
1086 acute cold exposure on norpinephrine turnover rates in rat white
1087 adipose tissue. *Journal of the Autonomic Nervous System* **60**:206–
1088 208. doi:10.1016/0165-1838(96)00037-9
- 1089 Grieve AG, Xu H, Künzel U, Bambrough P, Sieber B, Freeman M. 2017.
1090 Phosphorylation of iRhom2 at the plasma membrane controls

- 1091 mammalian TACE-dependent inflammatory and growth factor
1092 signalling. *eLife* **6**:1–22. doi:10.7554/eLife.23968
- 1093 Jendzjowsky NG, Roy A, Barioni NO, Kelly MM, Green FHY, Wyatt CN,
1094 Pye RL, Tenorio-Lopes L, Wilson RJA. 2018. Preventing acute
1095 asthmatic symptoms by targeting a neuronal mechanism involving
1096 carotid body lysophosphatidic acid receptors. *Nature*
1097 *Communications* **9**:1–15. doi:10.1038/s41467-018-06189-y
- 1098 Jendzjowsky NG, Roy A, Iftinca M, Barioni NO, Kelly MM, Herrington
1099 BA, Visser F, Altier C, Wilson RJA. 2021. PKC ϵ stimulation of
1100 TRPV1 orchestrates carotid body responses to asthmakines. *Journal*
1101 *of Physiology* **599**:1335–1354. doi:10.1113/JP280749
- 1102 Kanashiro A, Sônego F, Ferreira RG, Castanheira FVS, Leite CA,
1103 Borges VF, Nascimento DC, Cólón DF, Alves-Filho JC, Ulloa L,
1104 Cunha FQ. 2017. Therapeutic potential and limitations of cholinergic
1105 anti-inflammatory pathway in sepsis. *Pharmacological Research*
1106 **117**:1–8. doi:10.1016/j.phrs.2016.12.014
- 1107 Katayama PL. 2016. Adrenaline and the carotid body during
1108 hypoglycaemia: an amplifying mechanism? *Journal of Physiology*
1109 **594**:7161–7162. doi:10.1113/JP273238
- 1110 Katayama PL, Castania JA, Dias DPM, Patel KP, Fazan R, Salgado HC.
1111 2015. Role of Chemoreceptor Activation in Hemodynamic
1112 Responses to Electrical Stimulation of the Carotid Sinus in
1113 Conscious Rats. *Hypertension* **66**:598–603.
1114 doi:10.1161/HYPERTENSIONAHA.115.05316
- 1115 Katayama PL, Castania JA, Fazan R, Salgado HC. 2019. Interaction
1116 between baroreflex and chemoreflex in the cardiorespiratory
1117 responses to stimulation of the carotid sinus/nerve in conscious rats.
1118 *Autonomic Neuroscience: Basic and Clinical* **216**:17–24.
1119 doi:10.1016/j.autneu.2018.12.001

- 1120 Kim SJ, Fong AY, Pilowsky PM, Abbott SBG. 2018. Sympathoexcitation
1121 following intermittent hypoxia in rat is mediated by circulating
1122 angiotensin II acting at the carotid body and subfornical organ.
1123 *Journal of Physiology* **596**:3217–3232. doi:10.1113/JP275804
- 1124 Kline DD, King TL, Austgen JR, Heesch CM, Hasser EM. 2010. Sensory
1125 afferent and hypoxia-mediated activation of nucleus tractus solitarius
1126 neurons that project to the rostral ventrolateral medulla.
1127 *Neuroscience* **167**:510–527.
1128 doi:10.1016/j.neuroscience.2010.02.012
- 1129 Koshiya N, Guyenet PG. 1996. Tonic sympathetic chemoreflex after
1130 blockade of respiratory rhythmogenesis in the rat. *Journal of*
1131 *Physiology* **491**:859–869. doi:10.1113/jphysiol.1996.sp021263
- 1132 Kox M, Van Eijk LT, Zwaag J, Van Den Wildenberg J, Sweep FCGJ,
1133 Van Der Hoeven JG, Pickkers P. 2014. Voluntary activation of the
1134 sympathetic nervous system and attenuation of the innate immune
1135 response in humans. *Proceedings of the National Academy of*
1136 *Sciences of the United States of America* **111**:7379–7384.
1137 doi:10.1073/pnas.1322174111
- 1138 Kressel AM, Tsaava T, Levine YA, Chang EH, Addorisio ME, Chang Q,
1139 Burbach BJ, Carnevale D, Lembo G, Zador AM, Andersson U,
1140 Pavlov VA, Chavan SS, Tracey KJ. 2020. Identification of a
1141 brainstem locus that inhibits tumor necrosis factor. *Proceedings of*
1142 *the National Academy of Sciences of the United States of America*
1143 **117**:29803–29810. doi:10.1073/pnas.2008213117
- 1144 Kumar P, Prabhakar NR. 2012. Peripheral chemoreceptors: Function
1145 and plasticity of the carotid body. *Comprehensive Physiology* **2**:141–
1146 219. doi:10.1002/cphy.c100069
- 1147 Lankadeva YR, May CN, McKinley MJ, Neeland MR, Ma S, Hocking DM,
1148 Robins-Browne R, Bedoui S, Farmer DGS, Bailey SR, Martelli D,

- 1149 McAllen RM. 2020. Sympathetic nerves control bacterial clearance.
1150 *Scientific Reports* **10**:1–8. doi:10.1038/s41598-020-72008-4
- 1151 Li DJ, Evans RG, Yang ZW, Song SW, Wang P, Ma XJ, Liu C, Xi T, Su
1152 DF, Shen FM. 2011. Dysfunction of the cholinergic anti-inflammatory
1153 pathway mediates organ damage in hypertension. *Hypertension*
1154 **57**:298–307. doi:10.1161/HYPERTENSIONAHA.110.160077
- 1155 Li M, Galligan J, Wang D, Fink G. 2010. The effects of celiac
1156 ganglionectomy on sympathetic innervation to the splanchnic organs
1157 in the rat. *Autonomic Neuroscience: Basic and Clinical* **154**:66–73.
1158 doi:10.1016/j.autneu.2009.11.009
- 1159 Luise King T, Heesch CM, Clark CG, Kline DD, Hasser EM. 2012.
1160 Hypoxia activates nucleus tractus solitarii neurons projecting to the
1161 paraventricular nucleus of the hypothalamus. *American Journal of*
1162 *Physiology - Regulatory Integrative and Comparative Physiology*
1163 **302**. doi:10.1152/ajpregu.00028.2012
- 1164 Ma Y, Zhao S, Shen S, Fang S, Ye Z, Shi Z, Hong A. 2015. A novel
1165 recombinant slow-release TNF α -derived peptide effectively inhibits
1166 tumor growth and angiogenesis. *Scientific Reports* **5**:1–17.
1167 doi:10.1038/srep13595
- 1168 Malheiros-Lima MR, Silva JN, Souza FC, Takakura AC, Moreira TS.
1169 2020. C1 neurons are part of the circuitry that recruits active
1170 expiration in response to peripheral chemoreceptors activation. *eLife*
1171 **9**:1–23. doi:10.7554/eLife.52572
- 1172 Marcus NJ, Del Rio R, Schultz EP, Xia X-H, Schultz HD. 2014. Carotid
1173 body denervation improves autonomic and cardiac function and
1174 attenuates disordered breathing in congestive heart failure. *The*
1175 *Journal of Physiology* **592**:391–408.
1176 doi:10.1113/jphysiol.2013.266221
- 1177 Martelli D, Yao ST, Mckinley MJ, Mcallen RM. 2014. Reflex control of

- 1178 inflammation by sympathetic nerves, not the vagus. *Journal of*
1179 *Physiology* **592**:1677–1686. doi:10.1113/jphysiol.2013.268573
- 1180 McBryde FD, Abdala AP, Hendy EB, Pijacka W, Marvar P, Moraes DJA,
1181 Sobotka PA, Paton JFR. 2013. The carotid body as a putative
1182 therapeutic target for the treatment of neurogenic hypertension.
1183 *Nature Communications* **4**:1–11. doi:10.1038/ncomms3395
- 1184 Melo MR, Gasparini S, Speretta GF, Silva EF, Rodrigues Pedrino G,
1185 Menani J V, Zoccal DB, Colombari DSA, Colombari E. 2019.
1186 Importance of the commissural nucleus of the solitary tract in
1187 renovascular hypertension. *Hypertension Research* **42**:587–597.
1188 doi:10.1038/s41440-018-0190-6
- 1189 Mkrtchian S, Kåhlin J, Ebberyd A, Gonzalez C, Sanchez D, Balbir A,
1190 Kostuk EW, Shirahata M, Fagerlund MJ, Eriksson LI. 2012. The
1191 human carotid body transcriptome with focus on oxygen sensing and
1192 inflammation - a comparative analysis. *Journal of Physiology*
1193 **590**:3807–3819. doi:10.1113/jphysiol.2012.231084
- 1194 Morrison SF. 2001. Differential control of sympathetic outflow. *American*
1195 *Journal of Physiology - Regulatory Integrative and Comparative*
1196 *Physiology* **281**. doi:10.1152/ajpregu.2001.281.3.r683
- 1197 Mughrabi IT, Hickman J, Jayaprakash N, Thompson D, Ahmed U,
1198 Papadoyannis ES, Chang YC, Abbas A, Datta-Chaudhuri T, Chang
1199 EH, Zanos TP, Lee SC, Froemke RC, Tracey KJ, Welle C, Al-Abed
1200 Y, Zanos S. 2021. Development and characterization of a chronic
1201 implant mouse model for vagus nerve stimulation. *eLife* **10**:1–24.
1202 doi:10.7554/ELIFE.61270
- 1203 Murray K, Rude KM, Sladek J, Reardon C. 2021. Divergence of
1204 neuroimmune circuits activated by afferent and efferent vagal nerve
1205 stimulation in the regulation of inflammation. *Journal of Physiology*
1206 **599**:2075–2084. doi:10.1113/JP281189

- 1207 Nardocci G, Martin A, Abarzúa S, Rodríguez J, Simon F, Reyes EP,
1208 Acuña-Castillo C, Navarro C, Cortes PP, Fernández R. 2015. Sepsis
1209 progression to multiple organ dysfunction in carotid chemo/baro-
1210 denervated rats treated with lipopolysaccharide. *Journal of*
1211 *Neuroimmunology* **278**:44–52. doi:10.1016/j.jneuroim.2014.12.002
- 1212 Narkiewicz K, Ratcliffe LEK, Hart EC, Briant LJB, Chrostowska M, Wolf
1213 J, Szyndler A, Hering D, Abdala AP, Manghat N, Burchell AE, Durant
1214 C, Lobo MD, Sobotka PA, Patel NK, Leiter JC, Engelman ZJ,
1215 Nightingale AK, Paton JFR. 2016. Unilateral Carotid Body Resection
1216 in Resistant Hypertension: A Safety and Feasibility Trial. *JACC:*
1217 *Basic to Translational Science* **1**:313–324.
1218 doi:10.1016/j.jacbts.2016.06.004
- 1219 Neff RA, Mihalevich M, Mendelowitz D. 1998. Stimulation of NTS
1220 activates NMDA and non-NMDA receptors in rat cardiac vagal
1221 neurons in the nucleus ambiguus. *Brain Research* **792**:277–282.
1222 doi:10.1016/S0006-8993(98)00149-8
- 1223 Niewinski P, Janczak D, Rucinski A, Tubek S, Engelman ZJ, Piesiak P,
1224 Jazwiec P, Banasiak W, Fudim M, Sobotka PA, Javaheri S, Hart
1225 ECJ, Paton JFR, Ponikowski P. 2017. Carotid body resection for
1226 sympathetic modulation in systolic heart failure: results from first-in-
1227 man study. *European Journal of Heart Failure* **19**:391–400.
1228 doi:10.1002/ejhf.641
- 1229 Norlander AE, Madhur MS, Harrison DG. 2018. The immunology of
1230 hypertension *The Journal of Experimental Medicine* 21–34.
- 1231 Paxinos G, Charles Watson. 2007. *The Rat Brain in Stereotaxic*
1232 *Coordinates Sixth Edition*, Elsevier Academic Press.
- 1233 Pijacka W, Katayama PL, Salgado HC, Lincevicius GS, Campos RR,
1234 McBryde FD, Paton JFR, Schultz H, Powell F. 2018. Variable role of
1235 carotid bodies in cardiovascular responses to exercise , hypoxia and

- 1236 hypercapnia in spontaneously hypertensive rats **00**:1–16.
1237 doi:10.1113/JP275487
- 1238 Rauchhaus M, Doehner W, Francis DP, Davos C, Kemp M, Liebenthal
1239 C, Niebauer J, Hooper J, Volk HD, Coats AJS, Anker SD. 2000.
1240 Plasma cytokine parameters and mortality in patients with chronic
1241 heart failure. *Circulation* **102**:3060–3067.
1242 doi:10.1161/01.CIR.102.25.3060
- 1243 Schultz HD, Li YL, Ding Y. 2007. Arterial chemoreceptors and
1244 sympathetic nerve activity: Implications for hypertension and heart
1245 failure. *Hypertension* **50**:6–13.
1246 doi:10.1161/HYPERTENSIONAHA.106.076083
- 1247 Sesso HD, Jiménez MC, Wang L, Ridker PM, Buring JE, Michael
1248 Gaziano J. 2015. Plasma inflammatory markers and the risk of
1249 developing hypertension in men. *Journal of the American Heart*
1250 *Association* **4**:1–9. doi:10.1161/JAHA.115.001802
- 1251 Shin MK, Eraso CC, Mu YP, Gu C, Yeung BHY, Kim LJ, Liu XR, Wu ZJ,
1252 Paudel O, Pichard LE, Shirahata M, Tang WY, Sham JSK, Polotsky
1253 VY. 2019. Leptin Induces Hypertension Acting on Transient
1254 Receptor Potential Melastatin 7 Channel in the Carotid Body.
1255 *Circulation Research* **125**:989–1002.
1256 doi:10.1161/CIRCRESAHA.119.315338
- 1257 Shu HF, Wang BR, Wang SR, Yao W, Huang HP, Zhou Z, Wang X, Fan
1258 J, Wang T, Ju G. 2007. IL-1 β inhibits IK and increases [Ca²⁺]_i in the
1259 carotid body glomus cells and increases carotid sinus nerve firings in
1260 the rat. *European Journal of Neuroscience* **25**:3638–3647.
1261 doi:10.1111/j.1460-9568.2007.05586.x
- 1262 Simó R, Barbosa-Desongles A, Lecube A, Hernandez C, Selva DM.
1263 2012. Potential role of tumor necrosis factor- α in downregulating sex
1264 hormone-binding globulin. *Diabetes* **61**:372–382. doi:10.2337/db11-

- 1265 0727
- 1266 Steinman L. 2004. Elaborate interactions between the immune and
1267 nervous systems. *Nature Immunology* **5**:575–581.
1268 doi:10.1038/ni1078
- 1269 Tanaka S, Abe C, Abbott SBG, Zheng S, Yamaoka Y, Lipsey JE,
1270 Skrypnyk NI, Yao J, Inoue T, Nash WT, Stornetta DS, Rosin DL,
1271 Stornetta RL, Guyenet PG, Okusa MD. 2021. Vagus nerve
1272 stimulation activates two distinct neuroimmune circuits converging in
1273 the spleen to protect mice from kidney injury. *Proceedings of the
1274 National Academy of Sciences of the United States of America*
1275 **118**:1–12. doi:10.1073/PNAS.2021758118
- 1276 Thompson EL, Ray CJ, Holmes AP, Pye RL, Wyatt CN, Coney AM,
1277 Kumar P. 2016. Adrenaline release evokes hyperpnoea and an
1278 increase in ventilatory CO₂ sensitivity during hypoglycaemia: a role
1279 for the carotid body. *Journal of Physiology* **594**:4439–4452.
1280 doi:10.1113/JP272191
- 1281 Tromp TR, Mahesh D, Joles JA, Ramchandra R. 2018. Direct recording
1282 of cardiac and renal sympathetic nerve activity shows differential
1283 control in renovascular hypertension. *Hypertension* **71**:1108–1116.
1284 doi:10.1161/HYPERTENSIONAHA.117.10749
- 1285 van Maanen MA, Vervoordeldonk MJ, Tak PP. 2009. The cholinergic
1286 anti-inflammatory pathway: Towards innovative treatment of
1287 rheumatoid arthritis. *Nature Reviews Rheumatology* **5**:229–232.
1288 doi:10.1038/nrrheum.2009.31
- 1289 van Westerloo DJ, Choi G, Löwenberg EC, Truijien J, de Vos AF, Endert
1290 E, Meijers JCM, Zhou L, Pereira MPFL, Queiroz KCS, Diks SH, Levi
1291 M, Peppelenbosch MP, van der Poll T. 2011. Acute stress elicited by
1292 bungee jumping suppresses human innate immunity. *Molecular
1293 Medicine* **17**:180–188. doi:10.2119/molmed.2010.00204

- 1294 Wang X, Wang BR, Duan XL, Zhang P, Ding YQ, Jia Y, Jiao XY, Ju G.
1295 2002. Strong expression of interleukin-1 receptor type I in the rat
1296 carotid body. *Journal of Histochemistry and Cytochemistry* **50**:1677–
1297 1684. doi:10.1177/002215540205001213
- 1298 Watkins LR, Goehler LE, Relton JK, Tartaglia N, Silbert L, Martin D,
1299 Maier SF. 1995. Blockade of interleukin-1 induced hyperthermia by
1300 subdiaphragmatic vagotomy: evidence for vagal mediation of
1301 immune-brain communication. *Neuroscience Letters* **183**:27–31.
1302 doi:10.1016/0304-3940(94)11105-R
- 1303 Wei S, Zhang Z, Beltz TG, Yu Y, Johnson AK, Felder RB. 2013.
1304 Subfornical Organ Mediates Sympathetic and Hemodynamic
1305 Responses to Blood-Borne Proinflammatory Cytokines 118–125.
1306 doi:10.1161/HYPERTENSIONAHA.113.01404
- 1307 Willis A, Mihalevich M, Neff RA, Mendelowitz D. 1996. Three types of
1308 postsynaptic glutamatergic receptors are activated in DMNX neurons
1309 upon stimulation of NTS. *American Journal of Physiology -*
1310 *Regulatory Integrative and Comparative Physiology* **271**.
1311 doi:10.1152/ajpregu.1996.271.6.r1614
- 1312 Yuan G, Peng YJ, Khan SA, Nanduri J, Singh A, Vasavda C, Semenza
1313 GL, Kumar GK, Snyder SH, Prabhakar NR. 2016. H₂S production by
1314 reactive oxygen species in the carotid body triggers hypertension in
1315 a rodent model of sleep apnea. *Science Signaling* **9**:1–11.
1316 doi:10.1126/scisignal.aaf3204
- 1317 Zera T, Moraes DJA, da Silva MP, Fisher JP, Paton JFR. 2019. The
1318 Logic of Carotid Body Connectivity to the Brain. *Physiology* **34**:264–
1319 282. doi:10.1152/physiol.00057.2018
- 1320 Zhang ZH, Wei SG, Francis J, Felder RB. 2003. Cardiovascular and
1321 renal sympathetic activation by blood-borne TNF- α in rat: The role of
1322 central prostaglandins. *American Journal of Physiology - Regulatory*

1323 *Integrative and Comparative Physiology* **284**:916–927.

1324 doi:10.1152/ajpregu.00406.2002

1325

1326

1327

1328

1329

1330

1331

1332

1333

1334

1335

1336

1337

1338

1339

1340

1341

1342

1343

1344

1345

1346

1347

1348

1349

1350

1351

1352

1353

1354

1355

1356

1357

1358
1359
1360
1361
1362
1363

1364

1365
1366
1367
1368
1369
1370
1371
1372
1373
1374

1375

1376

1377

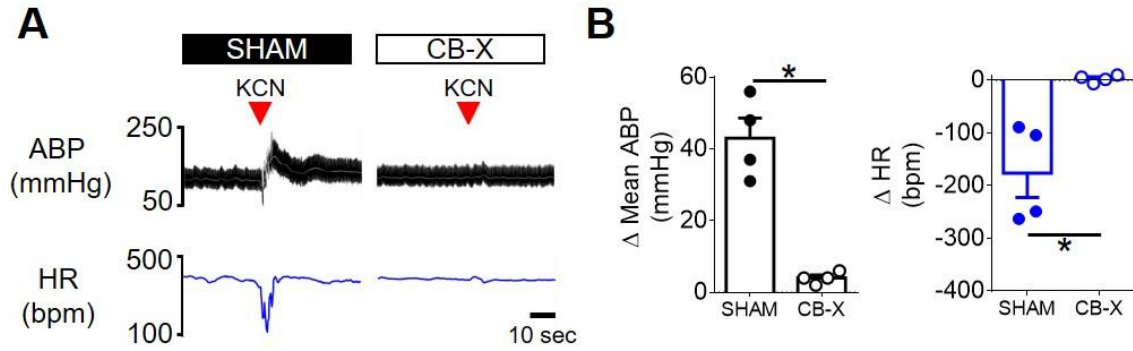
1378
1379
1380
1381
1382
1383
1384
1385
1386
1387
1388
1389
1390
1391
1392
1393
1394
1395

Supplementary Information

The Carotid Body Detects Circulating Tumor Necrosis Factor-Alpha to Activate a Sympathetic Anti-Inflammatory Reflex

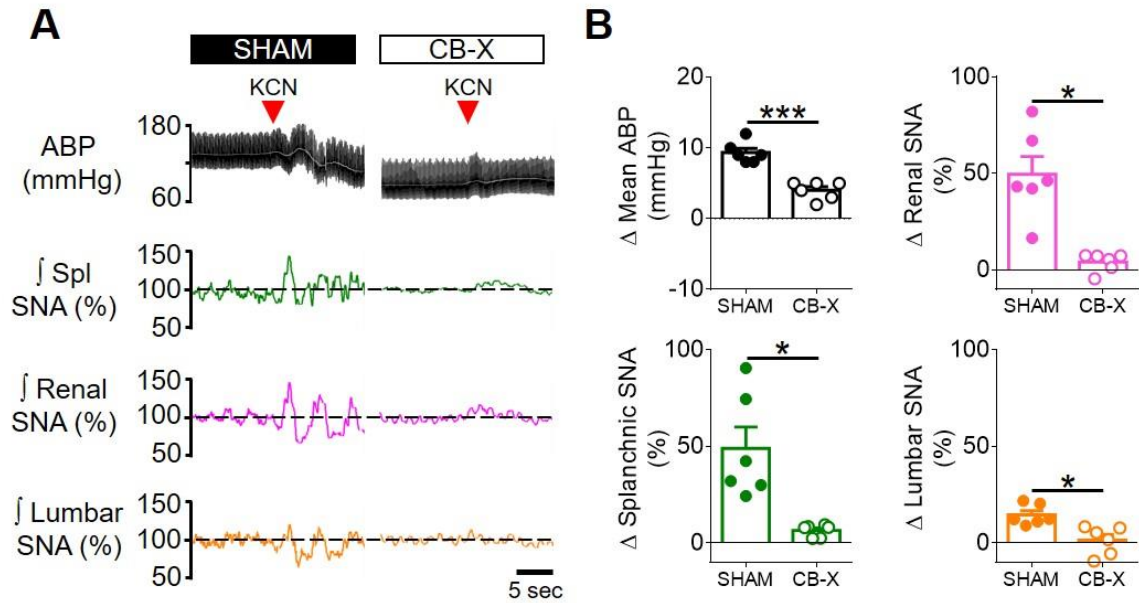
Pedro L. Katayama¹, Isabela P. Leirão¹, Alexandre Kanashiro², João Paulo M. Luiz², Fernando Q. Cunha², Luiz C. C. Navegantes³, Jose V. Menani¹, Daniel B. Zoccal¹, Débora S. A. Colombari¹ & Eduardo Colombari¹

Affiliations: ¹Department of Physiology and Pathology, School of Dentistry, São Paulo State University, Araraquara, São Paulo, Brazil. ²Department of Pharmacology, Ribeirão Preto Medical School, University of São Paulo, Ribeirão Preto, São Paulo, Brazil. ³Department of Physiology, Ribeirão Preto Medical School, University of São Paulo, Ribeirão Preto, São Paulo, Brazil.



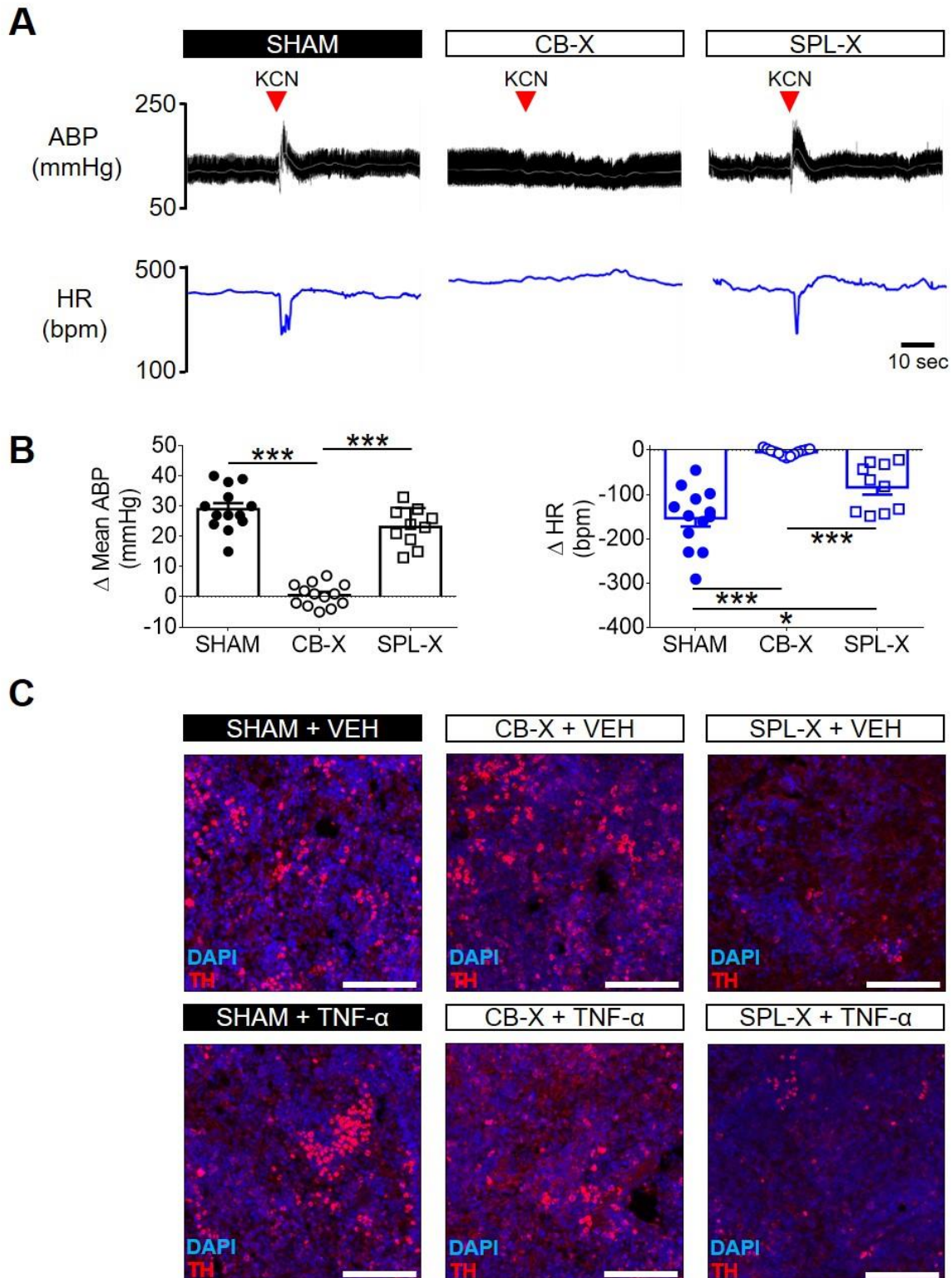
1396
1397
1398
1399
1400
1401
1402
1403
1404
1405
1406
1407
1408
1409
1410
1411
1412
1413
1414
1415
1416
1417
1418
1419
1420
1421
1422
1423
1424
1425
1426
1427

Figure supplement 1. Verification of carotid body ablation in *experiment 3*. **A.** Representative tracings of arterial blood pressure (pulsatile ABP, black; mean ABP, white) and heart rate (HR; blue) of a SHAM rat (left) and of a CB-X rat (right) in response to KCN (red arrowhead, 40 μ g, IV) under unanesthetized conditions. **B.** Summary data showing the peak changes in mean ABP and HR in response to KCN from SHAM (filled symbols, n = 4) and CB-X (open symbols, n = 4) rats. The cardiovascular responses to carotid body stimulation by intravenous KCN were abolished in CB-X rats, confirming the efficacy of bilateral carotid body ablation: Δ mean ABP (SHAM, 43 ± 6 mmHg; CB-X, 4 ± 1 mmHg; $t(3.128) = 6.912$, $p = 0.005$, Welch's *t*-test), Δ HR (SHAM, -176 ± 46 bpm; CB-X, 3 ± 3 bpm; $t(3.033) = -3.866$, $p = 0.03$, Welch's *t*-test). * $p < 0.05$. Data are means \pm SEM.



1428
1429
1430
1431
1432
1433
1434
1435
1436
1437
1438
1439
1440
1441
1442
1443
1444
1445
1446
1447
1448
1449
1450
1451
1452
1453
1454
1455
1456

Figure supplement 2. Verification of carotid body ablation at the end of *experiment 4*. **A.** Representative tracings of arterial blood pressure (pulsatile ABP, black; mean ABP, white), splanchnic SNA (Spl; green), renal SNA (magenta) and lumbar SNA (orange) of a SHAM rat (left) and of a CB-X rat (right) in response to KCN (red arrowhead, 40 μ g, IV) under anesthetized conditions. **B.** Summary data showing the changes in mean ABP, Splanchnic SNA, Renal SNA and Lumbar SNA in response to KCN from SHAM (filled symbols, n = 6) and CB-X (open symbols, n = 6) rats. For each rat, baseline rectified and integrated SNA was normalized to 100% and the peak changes in response to KCN were calculated. The sympathetic and blood pressure responses to KCN were significantly attenuated in CB-X rats, confirming the efficacy of bilateral carotid body ablation: Δ Spl SNA (SHAM, 48 ± 11 %; CB-X, 7 ± 1 %; $U = 0$, $z = -2.882$, $p = 0.002$, Mann-Whitney U -test), Δ Renal SNA (SHAM, 50 ± 9 %; CB-X, 4 ± 2 %; $t(5.452) = 4.815$, $p = 0.004$, Welch's t -test), Δ Lumbar SNA (SHAM, 15 ± 2 %; CB-X, 1 ± 3 %; $t(10) = 3.547$, $p = 0.005$, Student's t -test), and Δ Mean ABP (SHAM, 9 ± 1 mmHg; CB-X, 4 ± 1 %; $t(10) = 6.644$, $p < 0.001$, Student's t -test). * $p < 0.05$ and *** $p < 0.001$. Data are means \pm SEM.



1457
1458
1459
1460
1461
1462
1463
1464
1465
1466

Figure supplement 3. Verification of carotid body ablation and splanchnic sympathetic denervation in *experiment 5*. **A.** Representative tracings of arterial blood pressure (pulsatile ABP, black; mean ABP, white) and heart rate (HR; blue) of a SHAM rat (left), of a CB-X rat (middle), and of a SPL-X rat (right) in response to KCN (red arrowhead, 40 μ g, IV) under unanesthetized conditions. **B.** Summary data showing the peak changes in mean ABP (black graphs, left) and HR (blue graphs, right) in response to KCN from SHAM (filled circles, n = 13), CB-X (open circles, n = 13), and SPL-X (open squares, n = 10) rats. The cardiovascular (mean ABP and HR) responses to carotid body stimulation by intravenous KCN were abolished in CB-X rats, confirming the efficacy of bilateral carotid body ablation: Δ mean ABP (SHAM, 29 ± 2 mmHg; CB-X, 1 ± 1 mmHg; SPL-X, 23 ± 2) and Δ mean HR (SHAM, -154 ± 19 bpm;

1467 CB-X, -4 ± 2 bpm; SPL-X, -84 ± 17). Regarding Δ mean ABP, a one-way ANOVA detected statistically
1468 significant differences between groups, $F_{(2, 33)} = 83.134$, $p < 0.001$. Subsequent post hoc analysis with
1469 a Bonferroni adjustment revealed that the mean difference in Δ mean ABP between CB-X and SHAM
1470 rats was statistically significant (-28 mmHg, 95% CI $[-34, -23]$, $p < 0.001$) as well as the mean difference
1471 in Δ mean ABP between CB-X and SPL-X rats (-22 mmHg, 95% CI $[-29, -16]$, $p < 0.001$). Regarding Δ
1472 HR, a Welch ANOVA detected statistically significant differences between groups, $F_{(2, 14.078)} = 40.040$,
1473 $p < 0.001$. Games-Howell post hoc analysis revealed that the mean difference in Δ HR between CB-X
1474 and SHAM rats was statistically significant (149 bpm, 95% CI $[99, 200]$, $p < 0.001$) as well as the mean
1475 difference in Δ mean HR between CB-X and SPL-X rats (79 bpm, 95% CI $[33, 126]$, $p = 0.003$). In
1476 addition, the mean difference in Δ mean HR between SHAM and SPL-X rats was also statistically
1477 significant (-70 bpm, 95% CI $[-133, -7]$, $p = 0.029$). * $p < 0.05$ and *** $p < 0.001$. Data are means \pm SEM.
1478 **C.** Representative images of spleen sections from one animal of each group obtained at the end of
1479 *experiment 5* and processed for nuclear staining (DAPI, blue) and tyrosine hydroxylase (TH, red). Note
1480 that TH staining is substantially less pronounced in the animals subjected to splanchnic sympathetic
1481 denervation (SPL-X + VEH, upper right panel; and SPL-X + TNF- α , bottom right panel) as compared to
1482 SHAM (SHAM + VEH, upper left panel; and SHAM + TNF- α , bottom left panel) and CB-X (CB-X + VEH,
1483 upper middle panel; and CB-X + TNF- α , bottom middle panel). VEH, vehicle. Scale bars: 100 μ m.